Available online at www.sciencedirect.com
ScienceDirect
Chemical Geology 247 (2008) 133–153
CHEMICAL GEOLOGY INCLUDING ISOTOPE GEOSCIENCE
www.elsevier.com/locate/chemgeo

Geochemistry and magmatic history of eclogites and ultramafic rocks from the Chinese continental scientific drill hole: Subduction and ultrahigh-pressure metamorphism of lower crustal cumulates

Yongsheng Liu [a,b,*], Keqing Zong [a], Peter B. Kelemen [c], Shan Gao [a]

[a] State Key Laboratory of Geological Processes and Mineral Resources, Faculty of Earth Sciences, China University of Geosciences, Wuhan 430074, China
[b] State Key Laboratory of Continental Dynamics, Department of Geology, Northwest University, Xi'an 710069, China
[c] Department of Earth & Environmental Sciences, Columbia University, NY 10964-8000, USA

Received 17 January 2007; received in revised form 17 October 2007; accepted 19 October 2007

Editor: R.L. Rudnick

Abstract

Three distinct groups of eclogites (low-Mg–Ti eclogites, high-Ti eclogites and Mg-rich eclogites) and ultramafic rocks from the depth interval of 100–680 m of the Chinese Continental Scientific Drill Hole were studied. The low Mg#s (=100*molar Mg/(Mg+Fe)) (81–84%) and low Ni (1150–1220 ppm) and high $Fe_2O_3^{total}$ (13–15 wt.%) contents of ultramafic rocks suggest a cumulate origin. Mg-rich eclogites show middle and heavy REE enrichments, which could not be produced by metamorphic growth of garnet. Instead, if the rocks formed from a light REE enriched magma, there may be an igneous precursor for some garnets in their protolith. Alternatively, perhaps they formed from a light REE depleted magma without garnet. The high-Ti eclogites are characterized by unusually high $Fe_2O_3^{total}$ contents (up to 24.5 wt.%) and decoupling of high TiO_2 from low Nb and Ta contents. These features cannot be produced by concentration of rutile during UHP metamorphism (even for samples with TiO_2 > 4 wt.%) of high-Ti basalts, but could be attributed to crystal fractionation of titanomagnetite (for those with TiO_2 < ~4 wt.%) or titanomagnetite+ilmenite (for those with TiO_2 > ~4 wt.%). Thus, we suggest that protoliths of the high-Ti eclogites were titanomagnetite/ilmenite-rich gabbroic cumulates. As a whole, the low-Mg–Ti eclogites are geochemically complementary to the high-Ti eclogites, Mg-rich eclogites and ultramafic rocks, and could be metamorphic products of gabbroic/dioritic cumulates formed by high degree crystal fractionation. All these observations suggest that parental materials of the ultramafic rock-eclogite assemblage could represent a complete sequence of fractional crystallization of tholeiitic or picritic magmas at intermediate to high pressure, which were later carried to ultrahigh-pressure conditions during a continental collision event.
© 2007 Elsevier B.V. All rights reserved.

Keywords: CCSD; Eclogite; Ultramafic rock; Cumulate; Magmatic history

* Corresponding author. State Key Laboratory of Geological Processes and Mineral Resources, China University of Geosciences, Wuhan 430074, China. Tel.: +86 27 87483044; fax: +86 27 67885096.
E-mail addresses: yshliu@cug.edu.cn, yshliu@hotmail.com (Y. Liu).

0009-2541/$ - see front matter © 2007 Elsevier B.V. All rights reserved.
doi:10.1016/j.chemgeo.2007.10.016

1. Introduction

The nature and origin of the lower continental crust remains one of the most important areas of study in the Earth sciences because it bears directly on how the continents were and are presently being formed. Several, not necessarily mutually exclusive hypotheses have been put forward (Rudnick, 1992, 1995; Kelemen, 1995). One possibility for forming lower continental crust is that it represents the residue of melting pre-existing crust at lower crustal pressures. Such an origin could be associated with orogenic thickening and heating of the thickened lower crust. A second possibility is that the lower crust represents fragments of stacked oceanic lithospheres, such that continents grow by lateral accretion. A third possibility is that the lower crust is generated by magmatic underplating, that is, continents grow from the bottom up. A fourth possibility is that substantial proportions of lower and upper continental crust form simultaneously via single-stage, arc magmatism with concurrent delamination (Kelemen et al., 2003; Greene et al., 2006; Lee et al., 2006).

Granulite (Griffin and O'Reilly, 1986; Rudnick et al., 1986; Kempton and Harmon, 1992; Wendlandt et al., 1993) and eclogite xenoliths (Griffin et al., 1990; El Fadili and Demaiffe, 1999; Barth et al., 2002) carried in basaltic or kimberlitic magmas offer one window into the lower crust. However, one disadvantage of working with xenoliths is that they are generally tiny fragments of the deep lithosphere and therefore do not preserve any structural relationships. Furthermore, complete crystallization sequences associated with basaltic underplating are very rare, and the ultramafic part of a hypothetical underplated sequence is usually missing (Hermann et al., 2001; Zhou et al., 2005b).

In this paper, we turn our attention to studying a relatively large section of the lower crust sampled continuously by the Chinese Continental Scientific Drilling Project (CCSD) located in the southwest part of the Dabie–Sulu UHP metamorphic terrain. Our study is centered on the 0-680 m long main drill hole (CCSD-MH), which is mainly composed of eclogites. The eclogites are interlayered with a few amphibolites and gneisses, and overlie an ultramafic section (Fig. 1b) (Zhang et al., 2004, 2006b). The CCSD drill holes allow us to reconstruct the compositional structure of a deep lower crustal section by studying down-core geochemical variations, which might provide a relatively complete sequence of crystal fractionation. Such information can be used to shed light on the petrogenesis of the lower crust.

Many eclogites are enriched in TiO_2 in the Dabie–Sulu area (Jahn, 1998; Xu et al., 2004a; Zhang et al., 2004). To account for the petrogenesis of high-Ti eclogites, igneous cumulates (Jahn, 1998) or a Ti-rich gabbroic intrusion (Zhang et al., 2004) were suggested as protoliths. Tang et al. (2007) attributed Ti enrichment of the eclogites to relatively high proportions of cumulus ilmenite. Based on the negative correlations between

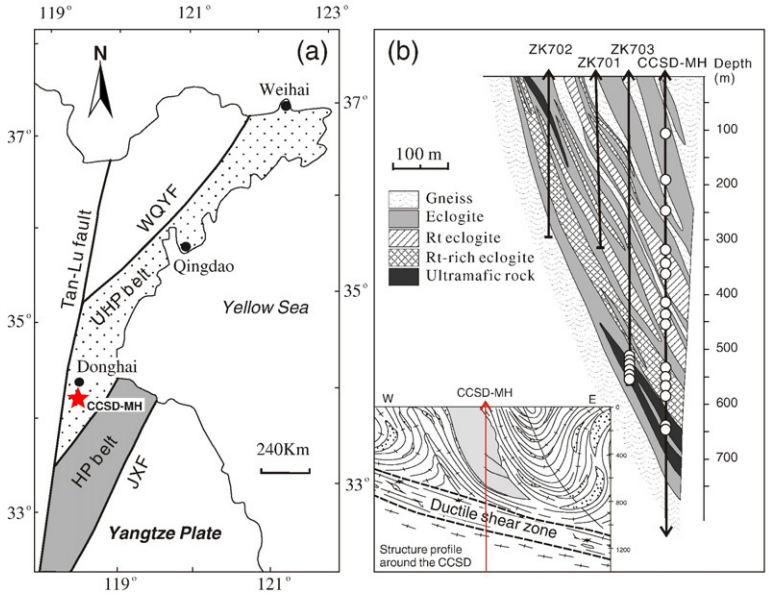

Fig. 1. (a) Simplified geological map of the Sulu area (modified from Zhang et al., 2000). WQYF = Wulian–Qingdao–Yantai fault, JXF = Jiashan–Xiangshui fault. (b) Profile around the CCSD-MH and ZK703 (Zhang et al., 2006a). The circles represent sample sites. Structure profile around the CCSD was revised from Xu et al. (2004b).

TiO_2 and Nb, Ta, Zr and Hf, we suggested that the protoliths of high-Ti eclogites were magnetite-bearing gabbroic cumulates (Liu et al., 2005c, 2007a; Zhang et al., 2006a). However, Liu et al. (2007a) suggested that some eclogites with $TiO_2 > 5$ wt.% must result from metamorphic enrichment in rutile rather than magmatic processes. Therefore, the origin of the samples with extremely high-Ti contents is still uncertain.

Specific questions that we wish to address in this study are as follows. First, what are the protoliths of the eclogites? Do these eclogites represent products of magmatic underplating or are they residues of partial melting? If the former, were all the eclogites formed by the same magmatic event? What were the protoliths of the ultramafic rocks underlying the eclogites? Are the high-Ti contents of eclogites inherited from their igneous protoliths or did they result from metamorphic differentiation? Finally, are the different types of eclogites and underlying ultramafic rocks genetically related, or juxtaposed by tectonic processes? Here, we present a new set of major and trace element data on whole rocks. The results show that the eclogite protoliths were probably gabbroic/dioritic cumulates. We show also that the ultramafic sections are cumulates, which were genetically related to the eclogites. Collectively, our findings suggest that parts of the Sulu terrane represent fragments of fossil lower crust formed by basaltic underplating, that were later affected by ultra-high pressure metamorphism during a continental collision event.

2. Geological setting

The Dabie–Sulu terrane in eastern-central China is located on the Triassic continental collision zone between the North China and Yangtze cratons. The Sulu UHP and HP metamorphic belts are bounded by the Wulian–Qingdao–Yantai and Jiashan–Xiangshui faults (Fig. 1a), and are the eastern extension of the Qingling–Dabie orogenic belts. Coesite is ubiquitous in eclogites from the Sulu UHP metamorphic belt (Liou and Zhang, 1996). Micro-diamonds have been found in eclogites from Donghai in the southwest end of the Sulu UHP metamorphic belt (Xu et al., 2003), where the CCSD-MH is located (34°25' N, 118 °40' E) (Fig. 1a). Many eclogites are enriched in Ti in this area (Xu et al., 2004a; Tang et al., 2007). Serpentinized peridotites and garnet pyroxenites occur sporadically as blocks throughout the UHP belt, most of which experienced UHP metamorphism (Liou and Carswell, 2000; Yang and Jahn, 2000; Zhang et al., 2003). At some localities, eclogites are directly associated with ultramafic rocks (e.g., Xugou).

The petrology of the CCSD-MH cores has been reported by Liu et al. (2004a,b) and Zhang et al. (2004, 2006b). The samples studied in this work were collected from 100 to 680 m of the CCSD-MH core (Fig. 1b), which were grouped into three lithological units by Zhang et al. (2004, 2006b). Unit 1 (from 100 to 530 m) consists mainly of quartz-rich eclogite, intercalated layers of rutile-rich eclogite and thin layers of paragneiss; Unit 2 (from 530 to 600 m) is mainly composed of rutile- and ilmenite-rich eclogites. Modal contents of titanomagnetite in these eclogites are high, up 5–25% (Xu et al., 2004a). Unit 3 (from 600 to 680 m) consists of ultramafic rock with minor eclogite and garnet clinopyroxenite layers. A 300 m thick ductile shear zone is found in the depth interval of 738–1100 m (Fig. 1b)(Xu et al., 2004b). Eclogites from the ductile shear zone have anomalously light oxygen isotope compositions (Zhang et al., 2006c; Chen et al., 2007).

The metamorphic P–T conditions are estimated to be 3.1–4.4 GPa and 678–816 °C for these eclogites (Zhang et al., 2006b). A protolith age of 774 Ma for the eclogites was suggested by Zhang et al. (2006a). Based on SHRIMP zircon U–Pb dating for orthogneiss, Liu et al. (2004a) suggested that these rocks underwent UHP metamorphism at 227 Ma and amphibolite facies retrograde metamorphism at 209 Ma. More recently, Liu et al. (2007b) found that trace element compositions (especially HREE) of the zircons from the ultramafic rocks change dramatically at ~255 Ma, and suggested that the UHP metamorphism occurred at 255–231 Ma, and retrograde metamorphism at about 227–192 Ma.

3. Samples and analytical methods

3.1. Sample description

Fifteen eclogite samples from the CCSD-MH (<680 m) were collected (Fig. 1b). The samples were classified into three types: low-Mg–Ti eclogites, high-Ti eclogites and Mg-rich eclogites. Low-Mg–Ti eclogites, sampled in the depth interval from 100–300 m, are mainly composed of garnet (grt)+omphacite (omp)+quartz+apatite (ap)+rutile (rut)±phengite. A few amphiboles are found as symplectite around garnet and omphacite in some samples, suggesting slight amphibolization. High-Ti eclogites, occurring in three layers in the depth interval from 300–610 m, are mainly composed of grt+omp+Ti–Fe oxides+ap. A few of them suffered slight amphibolization as demonstrated by amphibole symplectite around omphacite. Modal proportions of Ti–Fe oxides in high-Ti eclogites are about 8–16%. These oxides are composed of exsolution

lamellae of hematite (hem) + Ti-hematite + ilmenite (ilm) and rutile (Fig. 2a). Mg-rich eclogites are fresh and composed of omp + grt ± rut. They occur as lenses within the serpentinized ultramafic rocks in the depth interval from 610–680 m. Because ultramafic rocks from the CCSD-MH are not available, ultramafic rocks from ZK703 drill hole about 100 m away from CCSD-MH were analyzed for this study (Fig. 1b). The ultramafic samples from the ZK703 drill hole are thought to be counterparts of ultramafic rocks of the CCSD-MH based on petrologic features and VSP seismic profile (Zhang et al., 2006a). Olivines and pyroxenes are mostly serpentinized in the ultramafic rocks. Fresh garnets are preserved. A few of the garnets are euhedral and contain olivine and aluminous orthopyroxene inclusions (Fig. 2b).

3.2. Analytical methods

Parts of all samples were first crushed to about 60 mesh in a corundum jaw crusher. About 60 g was powdered in an agate ring mill to less than 200 mesh. Major elements were analyzed by X-ray fluorescene spectrometry (Rikagu RIX 2100) at the State Key Laboratory of Continental Dynamics, Northwest University, China (NU) and National Research Center for Geoanalysis, China (NRCG) (designated with italicized labels in Tables 1 and 2). Analytical precision and accuracy for major elements are the same as Rudnick et al. (2004) for the NU data and Zhang et al. (2004) for the NRCG data. Trace elements were analyzed by HR-ICP-MS (Finnigan Element 2) at Rice University for eclogites (Table 1) and ICP-MS at the China University of Geosciences for ultramafic rocks (Table 2). The samples were digested in Teflon bombs with a mixture of $HF + HNO_3$ for ICP-MS analyses (Appendix A). Analyses of international rock standards are listed in Appendix B.

4. Results

4.1. Eclogites

Based on modal mineralogies and $MgO–TiO_2$ variations (Fig. 3a), we classify the eclogites into three distinct groups: Mg-rich eclogites, high-Ti eclogites and low-Mg–Ti eclogites. Mg-rich eclogites ($MgO > 7.5$ wt.%) are characterized by high MgO contents and low TiO_2 contents. Compared to olivine gabbros, they have higher $Fe_2O_3^{total}$ and Na_2O contents and lower CaO contents. Their Ni and Cr contents are substantially higher than the other eclogites and most basaltic melts (e.g., MORB) (Fig. 4b and c). They show convex upwards light rare earth element (LREE) patterns, but flat heavy rare earth element (HREE) patterns and high HREE abundances (Fig. 5b).

High-Ti eclogites are characterized by high TiO_2 (2.8–5.9 wt.%), $Fe_2O_3^{total}$ (14.6–25.5 wt.%) and V (137–940 ppm) contents, and relatively low MgO and CaO contents (Figs. 3 and 4). $Fe_2O_3^{total}$ correlates positively with TiO_2 and V ($R = 0.72$ and 0.84, respectively) (Fig. 4d). Rare earth elements (REE) vary from highly LREE-depleted patterns for eclogites adjacent to Mg-rich eclogites to LREE-enriched patterns for eclogites neighboring low-Mg–Ti eclogites (Fig. 5c). P_2O_5 contents correlate positively with LREE (e.g., La; Fig. 4e), and negatively with Eu anomalies (Fig. 4f).

It is noteworthy that Nb, Ta, Zr and Hf are decoupled from Ti for the high-Ti eclogites (Fig. 6). These high-Ti

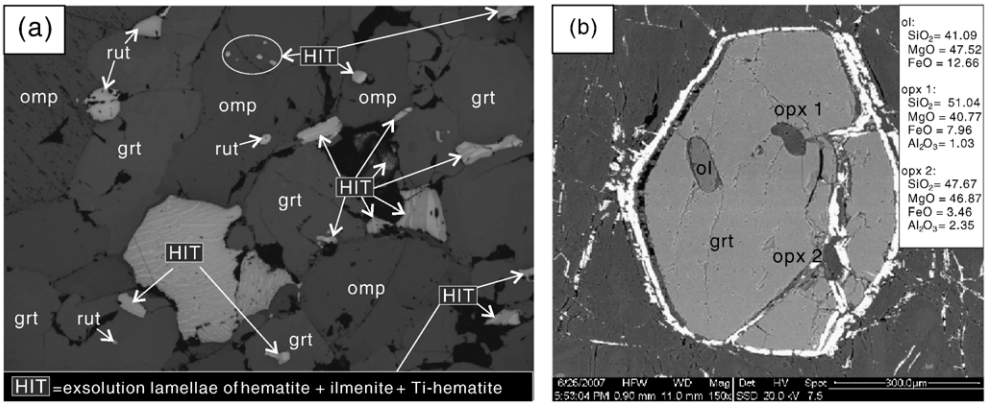

Fig. 2. (a) Distribution of Fe–Ti oxides in the high-Ti eclogite. (b) Euhedral garnet containing olivine and aluminous orthopyroxene inclusions. Units of olivine and pyroxene compositions are wt.%.

Table 1
Chemical compositions of eclogites (34°25' N, 118 °40' E)

Type	Low-Mg–Ti eclogite			High-Ti eclogite										Mg-rich eclogite	
Samples	SD001	SD004	SD006	SD009	SDZ1	SDZ2	SD014	SDZ3	SDZ4	SDZ5	SD017	SD018	SDZ6	SD019	SDZ7
Depth (m)	110	190	237	318	347	353	419	433	448	532	546	568	576	610	631
By XRF (wt.%)															
SiO_2	57.47	51.66	51.59	45.08	*43.34*	*40.33*	46.55	*47.42*	*40.24*	*42.25*	44.33	38.69	*39.16*	48.47	*45.85*
TiO_2	1.46	1.52	2.37	4.08	*5.63*	*4.40*	2.75	*3.37*	*5.85*	*4.44*	2.85	4.52	*3.45*	0.39	*1.37*
Al_2O_3	15.06	13.05	14.49	15.21	*14.28*	*14.97*	15.36	*14.57*	*11.47*	*14.37*	13.96	11.98	*18.11*	13.23	*14.95*
$Fe_2O_3^{total}$	11.25	13.05	14.46	16.54	*17.5*	*20.3*	16.48	*15.5*	*19.2*	*22.9*	15.34	24.47	*24.3*	10.99	*16.06*
MnO	0.34	0.19	0.28	0.24	*0.30*	*0.34*	0.23	*0.35*	*0.40*	*0.36*	0.23	0.26	*0.32*	0.16	*0.31*
MgO	1.96	5.76	4.12	7.37	*4.50*	*5.62*	5.29	*4.69*	*5.83*	*5.25*	7.15	7.30	*5.35*	12.42	*12.16*
CaO	5.14	10.10	7.74	9.03	*11.24*	*11.99*	9.36	*8.43*	*12.14*	*9.98*	12.05	11.11	*10.34*	9.85	*7.67*
Na_2O	5.73	3.95	3.12	2.21	*1.58*	*2.07*	3.63	*3.20*	*2.78*	*2.00*	2.96	1.28	*0.90*	3.76	*2.79*
K_2O	0.65	0.04	0.86	0.05	*0.00*	*0.13*	0.03	*1.08*	*0.06*	*0.02*	0.01	0.01	*0.08*	0.03	*0.06*
P_2O_5	0.46	0.30	0.70	0.22	*2.83*	*1.79*	0.26	*1.91*	*3.59*	*0.24*	0.63	0.02	*0.01*	0.02	*0.01*
LOI	0.41	0.33	0.19								0.04			0.33	
Total	99.93	99.95	99.92	100.0	101.2	101.9	99.93	100.5	101.6	101.8	99.54	99.64	102.0	99.65	101.2
By ICP-MS at the Rice University (units are wt.% for TiO_2, MnO and FeO, and ppm for the others)															
V	34.8	343	241	354	409	395	417	170	295	555	324	940	525	125	187
Cr	1.05	19.4	4.33	43.2		28.6	22.5	<0.003	<0.003	4.16	201	13.2	332	619	401
Be	1.11	1.10	0.90	0.22	0.48	0.46	0.80	1.15	0.78	0.55	0.24	0.063	0.12	0.74	0.66
Co	4.88	41.7	23.5	28.7	33.4	32.0	66.3	25.4	28.3	48.7	24.5	64.0	59.1	52.8	56.4
Ni	3.29	26.8	10.5	23.3	11.0	17.3	24.4	5.15	7.28	7.59	45.5	70.0	16.4	305	95.7
Cu	1.84	69.4	17.7	16.3	34.2	32.4	24.0	21.0	32.0	34.8	22.4	92.7	151	13.7	15.0
Zn	165	91.5	116	94.4	119	109	106	127	163	146	89.3	126	120	40.1	43.4
Ga	19.5	17.6	20.4	17.2	18.3	17.7	17.4	19.6	19.2	18.2	15.5	17.4	17.5	13.5	12.4
Rb	15.0	5.90	9.96	3.43	0.72	4.97	0.29	27.1	1.32	1.37	0.092	0.11	4.07	0.86	1.28
Sr	179	95.1	214	228	257	243	90.0	392	727	82.6	203	69.2	37.8	226	229
Y	59.7	36.7	48.3	10.7	55.2	38.5	34.6	66.8	64.3	35.5	19.0	10.8	10.8	30.7	83.3
Zr	430	108	252	10.4	88.4	31.8	101	93.4	49.3	77.0	36.0	12.8	11.0	102	293
Nb	10.1	4.31	6.40	0.71	4.46	2.16	5.05	5.35	4.71	3.02	1.53	0.39	0.31	2.93	7.07
Cs	1.03	0.20	0.38	0.031	0.004	0.10	0.060	0.79	0.013	0.46	0.028	0.028	0.25	0.17	0.14
Ba	149	199	392	17.9	6.65	25.6	11.8	304	19.7	70.9	1.62	4.90	49.1	99.5	16.8
La	19.9	6.25	24.6	6.69	59.9	21.4	3.98	26.0	29.0	4.81	3.89	0.55	0.091	3.14	7.78
Ce	54.3	18.4	66.6	16.4	151	64.7	8.66	70.2	80.8	11.0	11.6	2.01	0.38	12.0	22.0
Pr	7.44	3.13	9.51	2.38	17.0	8.15	1.06	9.22	10.5	1.50	1.81	0.38	0.11	1.89	3.34
Nd	34.9	16.8	45.1	11.6	72.5	39.8	4.97	46.9	52.7	7.84	10.2	2.30	1.22	9.13	15.9
Sm	8.19	5.17	10.8	2.65	16.4	9.16	1.94	11.9	14.3	2.57	3.04	1.19	1.21	2.74	4.53
Eu	3.76	2.06	4.37	1.17	4.82	3.16	1.01	4.75	5.40	1.36	1.40	0.72	0.89	0.80	1.15
Gd	10.4	5.78	11.8	2.99	15.8	8.99	3.70	12.9	15.2	3.42	3.83	1.57	1.24	3.46	5.62
Tb	1.73	0.97	1.79	0.44	2.34	1.27	0.77	1.93	2.15	0.64	0.60	0.27	0.22	0.62	1.11
Dy	11.1	6.43	9.87	2.46	11.5	6.80	5.57	10.9	11.5	4.54	3.91	1.86	1.50	4.61	8.65
Ho	2.49	1.53	1.90	0.48	1.79	1.24	1.35	2.21	2.08	1.18	0.83	0.43	0.38	1.18	2.52
Er	7.55	4.42	5.47	1.22	4.39	3.12	3.83	5.84	5.09	3.32	2.19	1.20	1.01	3.58	8.06
Tm	1.10	0.64	0.76	0.16	0.55	0.39	0.55	0.78	0.64	0.48	0.30	0.17	0.13	0.57	1.27
Yb	6.72	3.93	4.86	0.96	3.55	2.35	3.17	4.71	3.93	2.79	1.74	0.94	0.80	3.35	7.65
Lu	1.02	0.56	0.68	0.13	0.44	0.30	0.46	0.64	0.51	0.40	0.23	0.13	0.11	0.48	1.16
Hf	8.73	2.57	4.93	0.36	2.14	0.80	2.30	2.11	1.24	1.76	0.85	0.41	0.31	2.66	6.53
Ta	0.45	0.23	0.34	0.06	0.12	0.16	0.23	0.28	0.11	0.24	0.08	0.03	0.00	0.21	0.59
Pb	2.50	2.49	4.47	1.86	7.22	4.65	2.45	6.98	9.38	1.47	1.56	2.61	2.50	8.52	10.3
Th	1.27	0.42	2.08	0.25	10.4	4.27	0.68	2.55	2.48	0.48	0.12	0.09	0.02	0.15	0.54
U	0.46	0.23	0.58	0.07	1.62	0.56	0.45	0.66	0.55	0.18	0.06	0.06	0.09	0.09	0.22

Table 2
Compositions of the serpentinized ultramafic rocks from ZK 703 (34°25' N, 118°40'E)

Sample	703-521	703-526	703-535	703-541	703-545	703-545*
Depth (m)	521	526	535	541	545	545
By XRF (wt.%)						
SiO_2	37.22	37.11	36.57	36.99	36.54	36.71
TiO_2	0.19	0.21	0.19	0.29	0.29	0.28
Al_2O_3	4.11	4.44	3.37	3.70	3.19	3.21
$Fe_2O_3^{total}$	14.67	13.13	13.24	13.17	13.03	13.02
MnO	0.20	0.18	0.19	0.18	0.17	0.17
MgO	31.94	33.15	34.18	33.79	34.78	34.88
CaO	2.63	2.01	1.32	1.33	0.83	0.83
Na_2O	0.12	0.09	0.13	0.19	0.03	0.05
K_2O	0.01	<0.01	0.02	0.01	<0.01	0.01
P_2O_5	0.02	0.03	0.03	0.02	0.05	0.04
LOI	8.59	9.65	10.77	10.42	10.97	10.94
Total	99.69	100.00	100.01	100.09	99.88	100.14
Mg#	81.32	83.47	83.77	83.69	84.22	84.27
By ICP-MS at the China University of Geosciences (ppm)						
Be	0.067	0.095	0.096	0.099	0.084	
Sc	15.2	13.3	11.8	13.3	12.6	
V	51.7	54.7	61.5	68.3	72.3	
Cr	2236	2266	2123	2031	2129	
Co	123	126	134	132	136	
Ni	1151	1184	1219	1166	1201	
Cu	14.5	11.0	8.5	15.6	13.8	
Zn	88	70.4	69.4	69.2	70.6	
Ga	3.64	3.95	3.82	3.56	3.49	
Rb	0.017	0.00	0.366	0.00	0.69	
Sr	48.8	29.1	30.9	27.2	11.71	
Y	1.97	2.52	2.73	3.15	2.14	
Zr	4.94	6.85	5.39	6.83	5.99	
Nb	0.17	0.24	0.20	0.47	0.20	
Cs	0.009	0.007	0.069	0.011	0.018	
Ba	11.48	4.38	11.06	1.30	2.31	
La	0.49	0.47	0.74	0.67	1.16	
Ce	1.19	1.15	1.79	2.18	2.30	
Pr	0.17	0.16	0.25	0.33	0.28	
Nd	0.88	0.85	1.29	1.62	1.28	
Sm	0.27	0.30	0.37	0.44	0.32	
Eu	0.12	0.13	0.15	0.15	0.13	
Gd	0.31	0.36	0.41	0.47	0.34	
Tb	0.055	0.070	0.07	0.08	0.057	
Dy	0.33	0.42	0.45	0.51	0.33	
Ho	0.069	0.09	0.09	0.11	0.07	
Er	0.18	0.22	0.23	0.28	0.19	
Tm	0.027	0.035	0.034	0.044	0.030	
Yb	0.20	0.26	0.26	0.35	0.23	
Lu	0.030	0.040	0.040	0.056	0.035	
Hf	0.13	0.16	0.14	0.19	0.14	
Ta	0.060	0.061	0.051	0.08	0.065	
Pb	0.976	2.16	0.675	0.542	5.78	
Th	0.081	0.052	0.095	0.022	0.091	
U	0.023	0.013	0.021	0.009	0.023	

*duplicate.

eclogites have lower Nb, Ta, Zr and Hf contents than modern basalts (e.g., MORB) at similar TiO_2 levels. Similar features are also observed for oxide-rich gabbro xenoliths from the Hyblean Plateau (Scribano et al., 2006) and Indian Ocean spreading ridge gabbros (Hart et al., 1999; Coogan et al., 2001)(Fig. 6c).

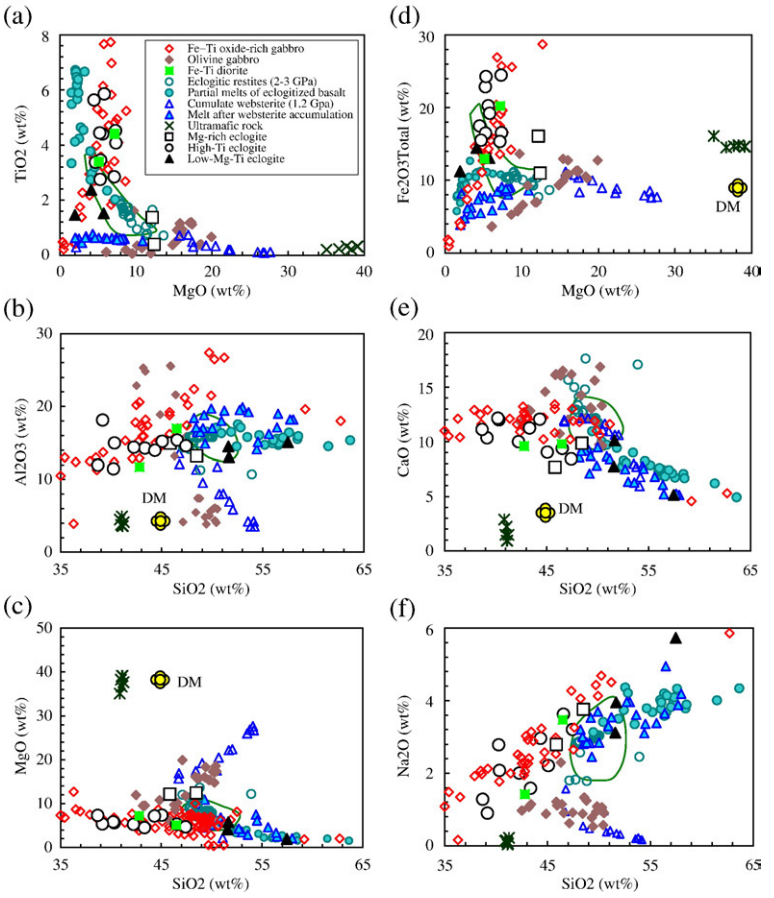

Fig. 3. Major-element diagrams illustrating geochemical relationships between eclogites, Fe–Ti oxide-rich gabbros (Zhou et al., 2005b), olivine gabbros (Liu et al., 2005a; Zhou et al., 2005a), Fe–Ti diorites (Hermann et al., 2001), cumulate websterites, and corresponding melts from high-pressure crystallization experiments of hydrous basalts and basaltic andesites (Müntener et al., 2001), eclogitic restites (reconstructed according to mass balance), and partial melts of eclogitized basalt (Pertermann and Hirschmann, 2003a,b). Ultramafic rocks were recalculated on an anhydrous basis. Solid outlined region represents field of mid-ocean ridge basalts (MORB) from RidgePetDB (Lehnert et al., 2000). Depleted mantle (DM) from (Salters and Stracke, 2004; Workman and Hart, 2005).

Low-Mg–Ti eclogites have relatively low TiO_2 (0.9–2.4 wt.%) and MgO (1.9–5.8 wt.%) contents and high SiO_2 (mostly 50–60 wt.%) and Na_2O (2.7–5.7 wt.%) contents (Fig. 3). Their V, Ni and Cr contents are lower than those of modern basalts (e.g. MORB) (Fig. 4). As a whole, V correlates positively with MgO (R=0.93, Fig. 4a). These eclogites have flat or LREE-enriched REE patterns with weak positive Eu anomalies (Fig. 5d). Although low-Mg–Ti eclogites have low TiO_2 contents, they have the highest Nb, Ta, Zr and Hf contents of any of our samples (Fig. 6).

4.2. Ultramafic rocks

The serpentinized ultramafic rocks are characterized by relatively low SiO_2 and CaO, and high $Fe_2O_3^{total}$ compared with depleted mantle (Fig. 3). Their Ni contents (1150–1220 ppm) and Mg#s (=100*molar Mg/(Mg+Fe)) (81–84%) are significantly lower than that expected for model depleted mantle (1960 ppm; Salters and Stracke, 2004; 1883 ppm; Workman and Hart, 2005) and lithospheric mantle peridotites (McDonough, 1990). Their REE patterns show enrichments in both LREE and HREE (Fig. 5a). One sample (703–541) demonstrates the typical convex upwards REE pattern for clinopyroxene-rich cumulates derived from a LREE-enriched magma.

5. Discussion

5.1. Effects of UHP metamorphism on trace elements

By comparing the high-grade metamorphic rocks to equivalent igneous rocks, Spandler et al. (2004) showed

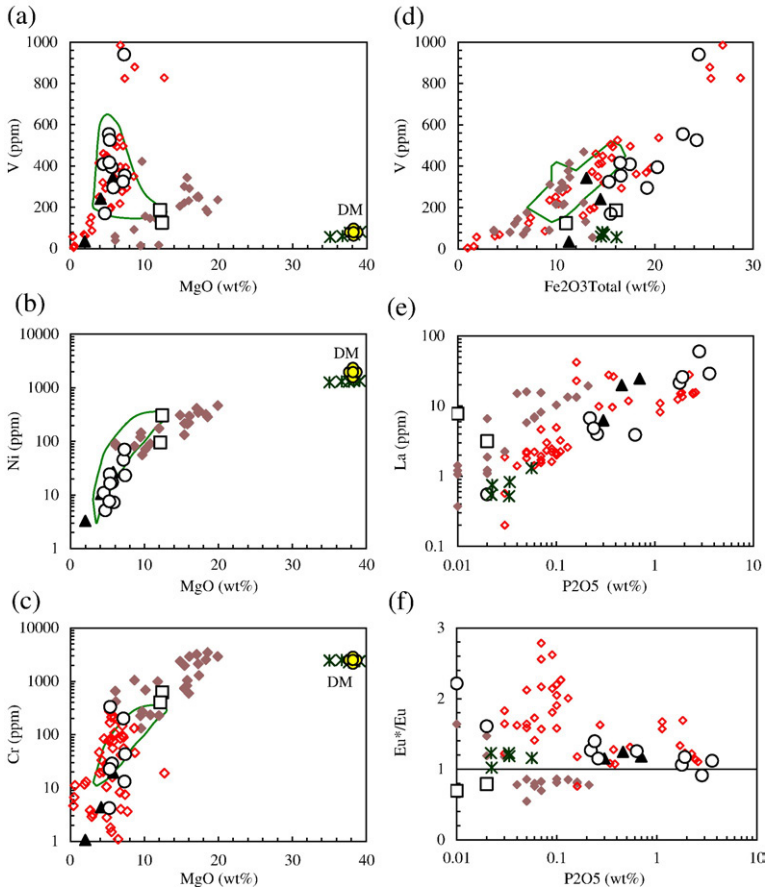

Fig. 4. Plots of MgO *vs.* V, Ni and Cr, and $Fe_2O_3^{total}$ *vs.* V, and P_2O_5 *vs.* La and Eu/Eu∗. DM = depleted mantle (Salters and Stracke, 2004; Workman and Hart, 2005). The other symbols as in Fig. 3.

that high-pressure metamorphism produced very minor chemical changes, with no significant mobility of high field strength elements (HFSE) and REE during subduction-zone metamorphism. Similar results were obtained from geochemical studies of high-pressure rocks from the Western Alps (Chalot-Prat et al., 2003). The degree of element mobility in subducted rocks depends significantly on thermal conditions in the slab and water content in the rocks. Crustal rocks subducted in a high temperature subduction-zone environment tend to undergo extensive depletion of incompatible trace elements by partial melting at fore-arc depths (Bebout et al., 1999; Becker et al., 2000). By contrast, exhumed fore-arc rocks from relatively cold subduction zones are relatively undepleted in trace elements (Bebout et al., 1999; Chalot-Prat et al., 2003; Spandler et al., 2004). If no partial melting occurred, trace element compositions of the rocks would not change significantly during the gabbro to eclogite transformation because trace elements are redistributed among the newly formed high-pressure major and accessory minerals (Miller et al., 2007). Dehydration of eclogites mainly affects the highly fluid-mobile elements (e.g., K, Rb, Cs, Ba), whereas elements such as Th, Nb, Ti, Zr, Nd, Sm and compatible elements show no evidence of significant losses (Becker et al., 2000).

Protoliths of the samples studied in this work could have been formed by basaltic underplating at the base of the lower crust as discussed below. There is no evidence indicating that they underwent pre-metamorphism alteration, and thus they may have contained negligible water prior to metamorphism. In addition, these rocks suffered a low temperature UHP metamorphism. Therefore, although the wet solidus for K-free MORB (Kessel et al., 2005) passes through the P–T conditions recorded by the Dabie–Sulu UHP rocks (Enami and Nagasaki, 1999; Zhang et al., 2000, 2006b; Mattinson et al., 2004), there is no evidence indicating widespread partial melting associated with UHP metamorphism. Most elements of the rocks probably were not affected by the

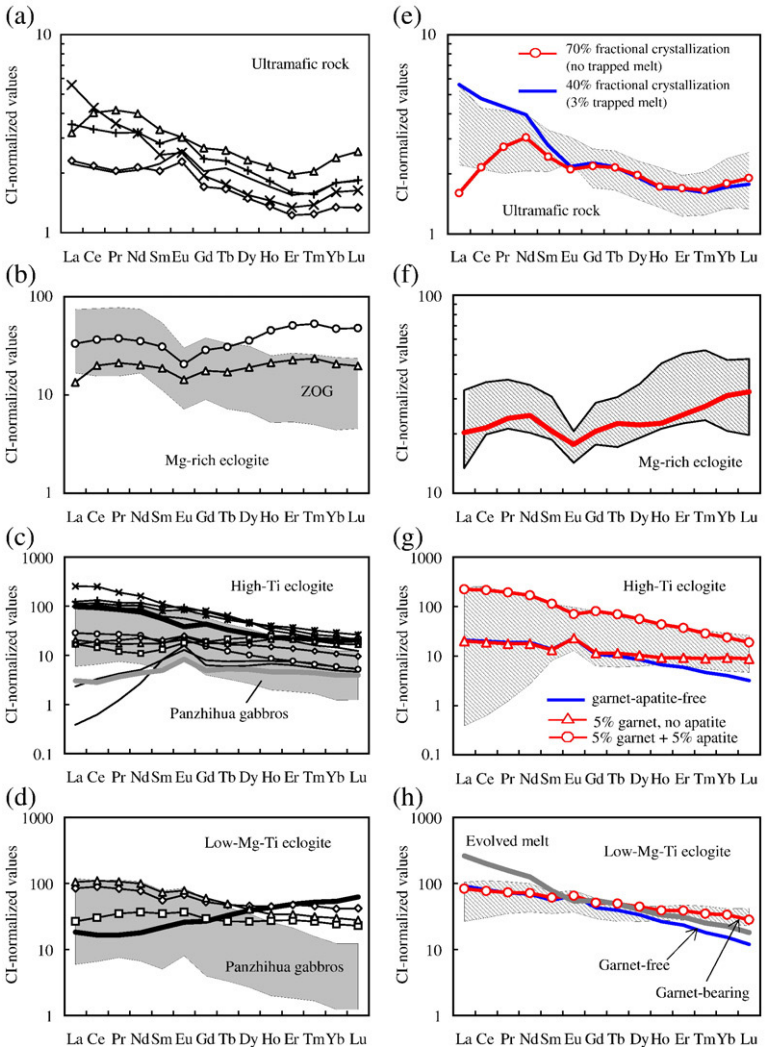

Fig. 5. (a–d) Chondrite (CI)-normalized REE patterns of eclogites and ultramafic rocks. CI values from McDonough and Sun (1995). The Zhujiapu (ZOG; Liu et al., 2005a) olivine gabbros and the Panzhihua high-Ti–Fe gabbros (Zhou et al., 2005b) are shown for comparison. Thick solid line and gray line in (c) are high-P_2O_5 Fe–Ti diorite (P_2O_5=0.45–0.87 wt.%) (Hermann et al., 2001) and low–P_2O_5 gabbro (P_2O_5<0.02 wt.%) (Giacomini et al., 2007). Thick solid lines in (d and h) are garnet diorite/tonalite from the Klanelneechina klippe (Kelemen et al., 2003). (e–h) REE patterns calculated according to fractional crystallization model. Parameters used in the calculations are listed in Tables 3 and 4.

UHP metamorphism. This is supported by the variations of fluid-mobile elements (e.g., K, Rb, Cs, Ba and Pb). Variations of Rb and Ba *vs.* K_2O for the eclogites are relatively similar to variations in modern MORB (Fig. 7), and differ from Cs, Pb and K variations produced during subduction-zone metamorphism (Bebout et al., 1999). These observations indicate that UHP metamorphism did not significantly affect the bulk chemical compositions of the rocks. Increasing Cs, Pb and Ba at low K_2O could be attributed to retrograde metamorphism, which introduced fluid and a few fluid-mobile elements. Therefore, we conclude that the main chemical variations of the rocks demonstrated by the fluid immobile elements (e.g., REE and HFSE) are mostly related to differences in their magmatic history.

5.2. Protoliths of serpentinized ultramafic rocks and eclogites

5.2.1. Serpentinized ultramafic rocks

Two hypotheses for the origin of ultramafic rocks are: (1) they are residual mantle peridotites, or (2) they are igneous cumulates, formed either by crystal fractionation or by reaction of fractionating melt with peridotite. Trace and major-element compositions of the ultramafic rocks do not match those of residual mantle

Table 3
Partition coefficients of minerals in basalt-andesite melts

	Partition coefficients[a]								
	Olivine	Clinopyroxene	Orthopyroxene	Garnet	Plagioclase	Amphibole	Apatite	Magnetite	Ilmenite
La	0.0004	0.054	0.002	0.01	0.075	0.12	14.5	0.015	
Ce	0.0005	0.098	0.003	0.021	0.062	0.24	21.1	0.016	
Nd	0.0010	0.21	0.0068	0.087	0.026	0.63	32.8	0.026	
Sm	0.0013	0.26	0.01	0.217	0.017	1.37	46	0.024	
Eu	0.0016	0.31	0.013	0.32	0.48	1.08	25.5	0.025	
Gd	0.0015	0.30	0.016	0.498	0.016	1.49	43.9	0.018	
Dy	0.0017	0.33	0.022	1.06	0.011	1.77	34.8		
Er	0.0015	0.30	0.03	2.00	0.0053	1.47	22.7		
Yb	0.0015	0.28	0.049	4.03	0.0041	1.15	15.4	0.018	
Lu	0.0015	0.28	0.06	5.50		1.07	13.8		
Ref.	M91	M91	M91	M91	D94	K97	F86	A90	
Ti	0.02	0.34	0.1	0.29	0.04			15	»1
Nb	0.01	0.004	0.15	0.003	0.03			1.3	2
Zr	0.012	0.119	0.18	0.27	0.0009			1.5	0.29
Ref.	U89	J98	U89	J98	D94			N94	Z98

[a] Ti, Nb and Zr partition coefficients of magnetite are selected based on negative correlations between $D_{Ti}^{magnetite}$ and TiO_2 contents of glass, and positive correlations between $D_{Nb,Zr}^{magnetite}$ and $D_{Ti}^{magnetite}$ (Nielsen et al., 1994; Nielsen and Beard, 2000). A90 = Agee (1990), D94 = Dunn and Sen (1994), F86 = Fujimaki (1986), J98 = Johnson (1998), K97 = Klein et al. (1997), M91 = McKenzie and O'Nions (1991), N94 = Nielsen et al. (1994), U89 = Ulmer (1989), Z98 = Zack and Brumm (1998).

Table 4
Model calculations of REE for eclogites and ultramafic rocks

	Starting material[a]	Ultramafic rock		Mg-rich eclogite	High-Ti eclogite			Low-Mg–Ti eclogite	
CI-normalized REE values									
La	97.1	5.63	1.60	20.2	20.9	20.1	222	91.6	83.7
Ce	74.8	4.78	2.16	21.4	19.8	18.8	214	80.7	77.1
Nd	49.7	3.96	3.05	24.7	18.8	17.8	168	69.0	72.0
Sm	31.9	2.78	2.44	20.6	13.5	13.3	113.2	55.9	61.0
Eu	23.0	2.18	2.11	17.6	23.0	23.1	69.9	66.4	65.3
Gd	24.1	2.27	2.19	20.5	10.83	11.53	80.3	43.0	51.0
Dy	19.3	1.93	1.97	22.1	8.45	10.30	55.5	33.7	44.4
Er	17.1	1.68	1.70	25.0	5.90	9.21	36.9	23.5	38.7
Yb	16.9	1.72	1.79	31.1	4.02	9.17	23.7	15.4	33.6
Lu	16.9	1.78	1.91	32.5	3.20	8.77	18.8	12.0	28.3
Fractional crystallization degree		40%	70%	40%	30%	30%	30%	70%	70%
Mineral proportions									
Trapped melt		3%		4%					
Olivine		65%	65%	5%					
Clinopyroxene		8%	8%	65%	45%	40%	35%	35%	35%
Orthopyroxene		20%	20%						
Garnet				30%		5%	5%		10%
Spinel		7%	7%						
Plagioclase					40%	40%	40%	60%	50%
Magnetite					15%	15%	15%		
Apatite							5%		
Amphibole								5%	5%

Partition coefficients used in the calculations were summarized in Table 3; Except for Mg-rich eclogite, garnet-free and garnet-bearing cumulates were calculated, respectively. The garnet-bearing cumulates match better with the eclogite samples than the garnet-free.

[a] Starting material is represented by the Neoproterozoic mafic volcanic rock from South China (Li et al., 2005).

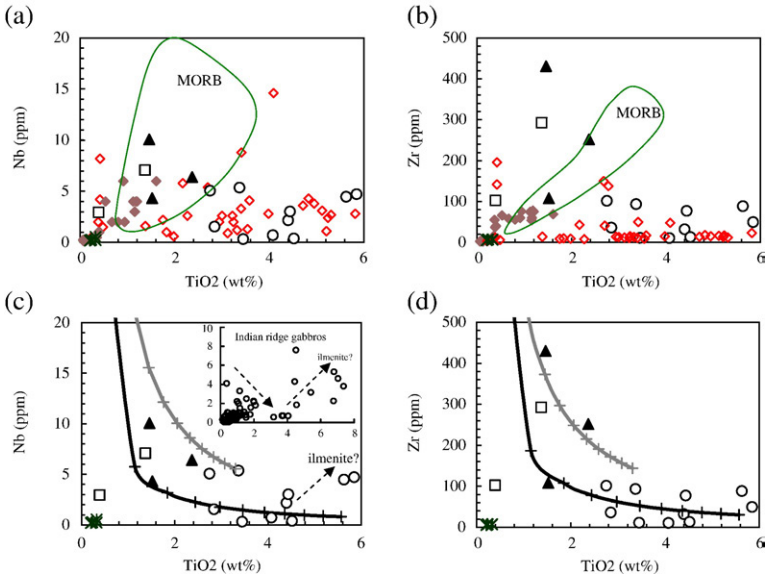

Fig. 6. Plots of TiO_2–Nb and–Zr for the eclogites. The dark and gray lines in (c) and (d) represent trends of cumulates (50%cpx+40%pl+10%mt) and corresponding melts formed by fractional crystallization involving titanomagnetite. Each tick on the lines represents 10% crystallization. Calculations were conducted assuming the initial melt has TiO_2=3 wt.%, Nb=5 ppm and Zr=130 ppm. Partition coefficients used in model calculation are listed in Table 3. The other symbols as in Fig. 3. Indian Ocean mid-ocean ridge gabbros from Hart et al. (1999) and Coogan et al. (2001).

peridotite. The ultramafic rocks analyzed for this study have significantly lower SiO_2 and Ni contents and Mg#s, and higher $Fe_2O_3^{total}$ contents, compared with lithospheric mantle peridotites (McDonough, 1990; Bodinier and Godard, 2003; Rudnick et al., 2004) and depleted mantle (Salters and Stracke, 2004; Workman and Hart, 2005)(Figs. 3 and 4). The highly variable CaO and MgO contents and low Mg#s are features of cumulates of olivine+clinopyroxene+orthopyroxene. An alternative interpretation is that these chemical

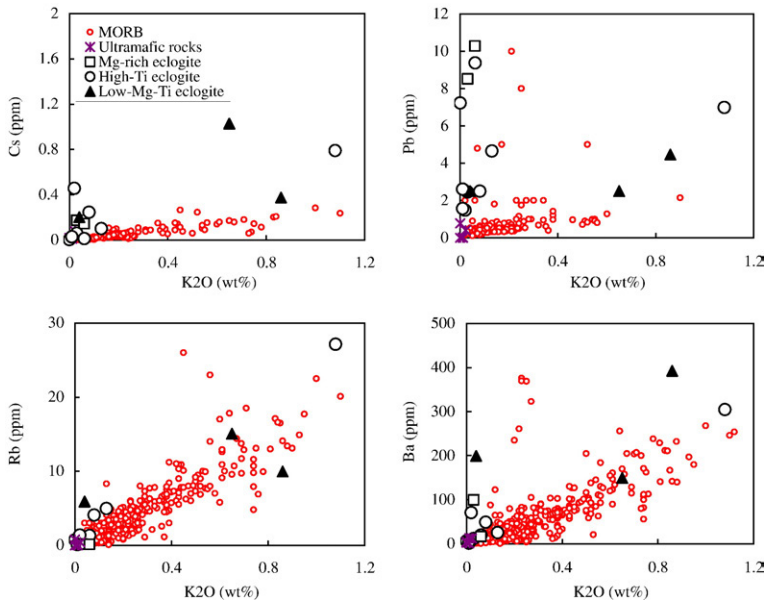

Fig. 7. Variations of K_2O *vs.* Cs, Pb, Rb and Ba of the samples. MORB is from RidgePetDB (Lehnert et al., 2000).

features resulted from pervasive weathering (Snow and Dick, 1995). However, the good correlation between MgO/SiO_2 and Al_2O_3/SiO_2 ratios ($R=-0.86$) suggests negligible weathering (Snow and Dick, 1995). Furthermore, CaO correlates negatively with MgO and such fluid immobile elements as V and Co ($R=-.95\sim-0.99$) (Menzies et al., 1993; Scambelluri et al., 2001), which would not be produced by serpentinization. However, mixing of olivine+clinopyroxene+orthopyroxene during crystal fractionation could produce cumulates with such features.

HFSE and REE are useful in inferring the petrogenesis of the serpentinized ultramafic rocks. As discussed above, it is generally suggested that no significant mobility of HFSE and REE occurs during subduction-zone metamorphism (Chalot-Prat et al., 2003; Spandler et al., 2004) and serpentinization processes (Menzies et al., 1993; Scambelluri et al., 2001). However, the recent study of Paulick et al. (2006) indicates that serpentinization could cause LREE enrichments and strong positive Eu anomalies, as seen in some abyssal peridotite. Sample 703-541 has the typical convex upwards REE pattern of clinopyroxene-bearing ultramafic cumulates derived from LREE-enriched magmas (Fig. 5a). The other four ultramafic samples show similar HREE patterns to 703-541, but different LREE patterns. These four samples are characterized by up-tilted La, Ce, Pr and Nd enrichments coupled with positive Eu anomalies. These features could be produced by either negligible trapped melt during formation of magmatic cumulates (Fig. 5e) or overprinting during serpentinization. Here, we use the correlations between LREE and Rb (mobile in aqueous fluid) and HFSE (mobile in melt) to distinguish between serpentinization and trapped melt. Except for 703-541, La, Ce, Pr and Nd correlate positively with Rb (correlation coefficients=0.90–0.99), but not with HFSE. These observations suggest that serpentinization could have contributed to the up-tilted La, Ce, Pr and Nd enrichments and positive Eu anomalies of most serpentinized ultramafic rocks.

In summary, we suggest that the protoliths of the serpentinized ultramafic rocks may have been igneous cumulates from basaltic magma. LREE may have been modified during serpentinization, except perhaps for sample 703-541 which preserves the igneous trace element characteristics of a cumulate from a LREE-enriched magma.

5.2.2. Mg-rich eclogites

Although the Mg-rich eclogites are hosted in serpentinized ultramafic rocks, the garnets in these eclogites are pyrope–almandine garnet, which are completely different from grossular-dominated garnets in eclogites with a rodingite protolith (Evans et al., 1981). These observations indicate that the protolith of the Mg-rich eclogites was not rodingitized gabbro associated with the serpentinized ultramafic rocks. Instead, we consider here three hypotheses for the parental materials of the Mg-rich eclogites: They could be (1) solidified melts, (2) residues of melting basaltic crust, or (3) igneous cumulates, from crystal fractionation or reaction of melt with peridotite.

The Mg-rich eclogites do not have major-element compositions matching primitive melt compositions. The SiO_2 and CaO contents are too low and MgO contents are too high for any known basaltic melts (Fig. 3). Their high Ni and Cr contents (Fig. 4) and convex upwards LREE patterns (Fig. 5b) preclude an origin as residues of melting pre-existing basaltic crust. Thus, we suggest that they have a cumulate origin.

Higher pressure (2–3 GPa) restites/cumulates from a tholeiitic magma would show a slight increase in MgO and CaO and a slight decrease in SiO_2 compared to the initial bulk composition, as shown in experiments (Pertermann and Hirschmann, 2003a,b) (Fig. 3). SiO_2 and CaO in our Mg-rich eclogites are too low and Na_2O is too high for these rocks to have been derived from melting or crystallization of tholeiitic parental material at high-pressure conditions (>2 GPa). Low pressure (<1 GPa) cumulates from basaltic magma would exhibit olivine control. Although the high Ni contents of our Mg-rich eclogites imply the presence of olivine in the protolith, their low MgO contents (8–17 wt.%) indicate that olivine was not the most abundant mineral. These Mg-rich eclogites have higher Al_2O_3 contents and lower MgO contents than websterites formed by partial crystallization/melting of basalt at 1.2 GPa (Müntener et al., 2001) (Fig. 3). Their SiO_2, Al_2O_3 and MgO variations suggest that garnet or plagioclase could have been abundant in the protolith.

Ni, Cr and MgO contents of Mg-rich eclogites are similar to the Zhujiapu and Tahe olivine gabbros (Fig. 4), which exhibit unequivocal cumulate textures (Liu et al., 2005a; Zhou et al., 2005a). However, the Mg-rich eclogites show higher $Fe_2O_3^{total}$ than the Zhujiapu and Tahe olivine gabbros for the same MgO contents (Fig. 3d). Thus, one possibility is that the Mg-rich eclogites were once olivine gabbros formed from high-Fe basaltic melts that were later metamorphosed into eclogite-phase assemblages by the Triassic UHP metamorphism. However, metamorphic growth of garnet could not produce the observed middle and HREE enrichments of the whole rocks. Assuming that the Mg-rich eclogites formed from a LREE-enriched magma such as the Proterozoic basalts of South China (Li et al., 2005), the relative middle and heavy REE

enrichments in the Mg-rich eclogites compared to the olivine gabbros (Fig. 5b) suggest that some garnets in the Mg-rich eclogites may have had an igneous precursor. Alternatively, perhaps the Mg-rich eclogites formed from a LREE-depleted magma, similar to MORB, in which case the relative enrichments of middle and heavy REE would be a consequence of the liquid composition and no garnet would be required. Because the spatially associated ultramafic cumulates seem to have formed from a LREE-enriched magma, we prefer the hypothesis that the Mg-rich eclogites also formed from a LREE-enriched magma and do include igneous garnet.

Igneous garnet could be formed by fairly high-pressure crystallization of basaltic magma, or by melt–peridotite reaction during continental subduction. Garnet-bearing igneous cumulates from basaltic melts at high pressure (crust–mantle boundary) have been observed in natural systems (Day et al., 1992; Ringuette et al., 1999; Harangi et al., 2001; Kelemen et al., 2003; Berger et al., 2005, 2007; Egorova et al., 2006) and crystallized in igneous crystallization experiments at 1.2 GPa (Müntener et al., 2001; Müntener and Ulmer, 2006). Alternatively, the protoliths of these Mg-rich eclogites were formed by melt–ultramafic cumulate reaction during the UHP metamorphism. Melt–peridotite reactions forming garnet pyroxenite have been observed in experiments (Rapp et al., 1999; Yaxley, 2000) and natural systems (Liu et al., 2005b). Both processes could produce pyroxenites with igneous garnet signatures (i.e. middle and heavy REE enrichments).

5.2.3. High-Ti eclogites

Most high-Ti eclogites are characterized by abundant rutile. However, the unusually low Nb, Ta, Zr and Hf contents in our samples, decoupled from high-Ti contents, indicate that Ti-enrichments were not produced by metamorphic differentiation, concentrating rutile that formed during the UHP metamorphism, because $D^{\mathrm{Rutile}}_{\mathrm{HFSE}}$ values are » 1 (Green and Pearson, 1987; Jenner et al., 1993; Foley et al., 2000; Schmidt et al., 2004; Klemme et al., 2005; Xiong et al., 2005). Furthermore, metamorphic differentiation only has a very local effect. Trace element compositions of the rocks would not change significantly during the gabbro/basalt to eclogite transformation (Miller et al., 2007). Thus, we consider two other alternative protoliths for the high-Ti eclogites: (1) high-Ti basalts, (2) igneous cumulates involving Ti–Fe-oxides.

Ti, Nb, Ta, Zr and Hf are all incompatible elements under normal mantle conditions. Thus, TiO_2 always correlates positively with Nb, Ta, Zr and Hf for basaltic magmas (e.g., MORB) (Fig. 6). However, the high-Ti eclogites we studied show remarkably low Nb, Ta, Zr and Hf contents, decoupled from the high-Ti contents. Furthermore, most of the high-Ti eclogites have extremely high $Fe_2O_3^{\mathrm{total}}$ contents (up to 23–25 wt.%), higher than any high-Ti basalts. These observations preclude high-Ti basalts as protoliths for the high-Ti eclogites.

Lower crustal gabbroic xenoliths with igneous texture from the Hyblean Plateau show chemical features (e.g., high Fe and Ti contents but low Nb and Ta contents) that are similar to the high-Ti eclogites (Scribano et al., 2006). Thus, we suggest that the parental materials of high-Ti eclogites may be igneous cumulates including abundant Ti–Fe-oxides, crystallized from an evolved magma.

The high-Ti eclogites show similar REE patterns and SiO_2–MgO, –Al_2O_3, MgO–TiO_2, $Fe_2O_3^{\mathrm{total}}$–TiO_2, –V and TiO_2–Nb, –Zr variations to the Panzhihua high-Ti gabbroic layered intrusions associated with Fe–Ti–V oxide deposits, which crystallized from evolved ferrobasaltic magmas (Zhou et al., 2005b). Thus, it is possible that the protoliths of high-Ti eclogites could be Ti–Fe-oxide-rich cumulates crystallized from highly evolved ferrobasaltic magma. This is consistent with the positive correlation between $Fe_2O_3^{\mathrm{total}}$ and V, extremely high $Fe_2O_3^{\mathrm{total}}$ and V contents, and low MgO, Cr and Ni contents in the high-Ti eclogites (Fig. 4a–d).

The variation of LREE concentrations of high-Ti eclogites cannot be the result of crystal fractionation of plagioclase, clinopyroxene and Ti–Fe-oxides alone, but could be related to some LREE-rich accessory minerals (e.g., apatite). LREE are far more compatible in apatite than in clinopyroxene and plagioclase (Paster et al., 1974; Hack et al., 1994; McKay et al., 1994; Bindeman et al., 1998; Prowatke and Klemme, 2006). A small fraction of apatite could significantly contribute to the LREE budget of the whole rock (Fig. 5g). The LREE-enriched eclogites have REE patterns similar to apatite-rich Fe–Ti diorites/gabbros (Hermann et al., 2001), whereas the LREE-depleted eclogites show similar REE patterns to the apatite-free cumulate gabbros (Giacomini et al., 2007) (Fig. 5c). Moreover, crystal fractionation of apatite can explain the highly variable P_2O_5 contents (0.01–3.59 wt.%) and positive correlation between La and P_2O_5 in the high-Ti eclogites (Fig. 4e). The positive Eu anomaly produced by cumulate plagioclase might be 'compensated' by a negative Eu anomaly in apatite to some degree, which could result in the negative correlations between P_2O_5 and Eu anomalies of the high-Ti eclogites (Fig. 4f).

5.2.4. Low-Mg–Ti eclogites

The low-Mg–Ti eclogites are geochemically complementary to the high-Ti eclogites and Mg-rich eclogites (Figs. 3–6). Compared to silicate melts in equilibrium with websterite (Fig. 3), low-Mg–Ti eclogites have lower Al_2O_3 contents, which imply that their parental materials underwent fractional crystallization of plagioclase and/or garnet. These features suggest that the protoliths of low-Mg–Ti eclogites were either solidified evolved melts or products of high degree crystal fractionation of evolved melts after crystal fractionation of olivine, pyroxene, garnet/plagioclase and titanomagnetite, which formed the protoliths of serpentinized ultramafic rocks, Mg-rich eclogites and high-Ti eclogites.

Solidified evolved melt after crystal fractionation of plagioclase would be characterized by a negative Eu anomaly. The weak positive Eu anomalies of low-Mg–Ti eclogites (Fig. 5d) imply that they could include a "cumulate" plagioclase component, and preclude them to be entirely composed of solidified evolved melts. Although the low-Mg–Ti eclogites have similarly high Al_2O_3 and CaO contents to the Panzhihua anorthosites, they have significantly higher HREE and HFSE contents than the anorthosites (Zhou et al., 2005b). Compared to the Panzhihua gabbros ($(La/Yb)_N=7.1$), the low-Mg–Ti eclogites ($(La/Yb)_N=2.3$) are more enriched in HREE (Fig. 5d). HREE contents of the low-Mg–Ti eclogites are close to garnet diorites and tonalites from the Klanelneechina klippe (Fig. 5d), which were interpreted as lower crustal cumulate or residual with igneous garnet (Kelemen et al., 2003). All the above observations make us speculate that the protoliths of low-Mg–Ti eclogites could be (garnet-bearing) diorite, which were derived from evolved melts after crystal fractionation of olivine, pyroxene, plagioclase/garnet and titanomagnetite.

5.3. Decoupling of Nb (Zr) from TiO2 in high-Ti eclogites

Crystallization of both magnetite and ilmenite can yield cumulates with high $Fe_2O_3^{total}$, V and TiO_2 contents. Very little ilmenite (<2%) is required to produce the decoupling of low Nb (Zr) contents from high-Ti contents for the high-Ti eclogites with TiO_2 ~ 4 wt.%. However, cumulate ilmenite alone could not explain the unusually high Fe contents of the high-Ti eclogites. Ilmenite-rich rocks possess not only high Fe_2O_{3total} and TiO_2 contents, but also high Nb and Zr contents (e.g., Fe–Ti–P rich diorite in the Braccia gabbro complex; Hermann et al., 2001). Samples with TiO_2 > ~4 wt.% could have a substantial amount of cumulus ilmenite, which show similar positive correlations between TiO_2 and Nb (Zr) to the Indian Ocean mid-ocean ridge gabbros (Fig. 6) (Hart et al., 1999; Coogan et al., 2001).

Magnetite can fractionate Nb (Zr) from Ti because $D^{magnetite/basalt}_{(Zr,\,Nb\,and\,Ta)}$ values correlate positively with $D^{magnetite/basalt}_{Ti}$ values, and $D^{magnetite/basalt}_{(Zr,\,Nb\,and\,Ta)}$ are <1 when $D^{magnetite/basalt}_{Ti}$ is <13 (Nielsen et al., 1994). The decoupling of low Nb (Zr) contents from high-Ti contents for high-Ti eclogites with TiO_2 < ~4 wt.% can be explained by accumulation of 50% cpx + 40%pl + 10%mt from a high-Ti basaltic magma (Fig. 6c and d). This is consistent with the presence of abundant titanomagnetite (5–25%) in the high-Ti eclogites (Xu et al., 2004a), most of which have decomposed into exsolution lamellae of hematite + Ti-hematite + ilmenite (Fig. 2a). Furthermore, it is noteworthy that the melts after fractional crystallization of magnetite-rich gabbros would possess high Zr (Nb) contents but low Ti contents, which are geochemical characteristics of the low-Mg–Ti eclogites (Fig. 6).

The TiO_2-rich compositions could be formed as a result of ilmenite crystallization during high-pressure (1.0 GPa) fractionation of gabbros, as demonstrated by experiments (Villiger et al., 2004). Precipitation of magnetite/ilmenite from silicate melts depends mainly on the overall Fe contents and Fe_2O_3/FeO ratios of the liquids (Reynolds, 1985). Fractional crystallization of olivine, pyroxene and plagioclase would increase the overall Fe content and Fe_2O_3/FeO ratio (and thus oxygen fugacity) of the basaltic magma. Magnetite saturation could occur in ferro-basaltic magmas when magma fO_2 was slightly above the FMQ buffer (Toplis and Carroll, 1996). Both primary ilmenite (Desmurs et al., 2002) and titanomagnetite (Coogan et al., 2001) have been observed in Fe–Ti-rich gabbros formed by low pressure igneous crystallization in oceanic environments. On the other hand, primary titanomagnetite and ilmenite were also observed in garnet-bearing cumulates (Berger et al., 2005; Egorova et al., 2006) and garnet-free gabbroic cumulates (Hermann et al., 2001; Greene et al., 2006; Scribano et al., 2006), both of which were interpreted as differentiation products of mafic magma at the continental crust-mantle boundary.

5.4. Modeling of the petrogenesis of the eclogite + ultramafic rock assemblage

As discussed above, the protoliths of the eclogite + ultramafic rock assemblage could have been formed by fractional crystallization from a LREE-enriched mafic magma. To test the hypothesis, crystallization processes

were modeled using REE based on the following assumptions (Fig. 5e–h; Table 4):

(1) The parental melt had the composition of the Neoproterozoic mafic volcanic rocks from South China (Li et al., 2005) (Table 4).
(2) Protoliths of the ultramafic rocks are olivine (ol)+orthopyroxene (opx)+clinopyroxene (cpx)+spinel cumulates, ±trapped melt (TM).
(3) Protoliths of the Mg-rich eclogites are cpx+garnet (grt)+ol cumulates, ±TM.
(4) Protoliths of the high-Ti eclogites are cpx+pl+magnetite (mag)±apatite (ap)±grt cumulates, ±TM.
(5) Protoliths of low-Mg–Ti eclogites are solidified evolved melt remaining after crystal fractionation steps (2) through (4), or dioritic/gabbroic cumulates (pl+cpx+amp±grt±TM).

HREE and MREE patterns of serpentinized ultramafic rocks can be well modeled by ~40% fractional crystallization of ol+opx+cpx+sp+2%TM or ~70% fractional crystallization of ol+opx+cpx+sp (Fig. 5e). Their enriched LREE patterns could be produced by 2% trapped melt or overprinting during serpentinization as discussed above.

Calculated garnet-bearing cumulates are more similar to the samples than garnet-free cumulates for the eclogites (Fig. 5f–h). Mg-rich eclogites can be roughly modeled by fractional crystallization of cpx+grt+ol with 4% trapped melt (Fig. 5f), although we cannot fit the flat middle- to heavy REE pattern observed in the samples using the same initial melt composition used for modeling ultramafic cumulates. Using a different initial melt (HREE depleted rather than the flat middle to heavy REE melt composition used in modeling ultramafic cumulates), the entire REE pattern of the Mg-rich eclogites can be matched with the same mineral proportions.

Except for the two samples with extremely low LREE, the remarkably variable REE patterns of high-Ti eclogites can be well modeled as apatite-bearing gabbroic cumulates (Fig. 5g), which is consistent with the highly variable P_2O_5 contents of these eclogites (e.g., correlation of P_2O_5 with La in Fig. 4e). The two samples with extremely low LREE could be affected by local metamorphic differentiation.

The low-Mg–Ti eclogites do not match evolved melt remaining after crystal fractionation steps (2) through (4), but are similar to garnet-bearing gabbroic/dioritic cumulates formed by ~70% crystal fractionation (Fig. 5h). The residual melt shows negative Eu anomaly and much higher LREE and lower HREE contents than the low-Mg–Ti eclogites.

5.5. Lower crustal growth associated with basaltic underplating

Oxygen isotope compositions of the eclogite units investigated in this work were reported by Zhang et al. (2006c; $\delta^{18}O = 0 \sim 6$) and Chen et al. (2007; $\delta^{18}O$ are dominated by $-6 \sim 0$). The remarkable difference between the two dataset implies that the oxygen isotope compositions are significantly heterogeneous (assuming both data are correct), and the original oxygen isotopic features could have been partially reset during UHP metamorphism and exhumation. This is confirmed by the gradual decrease of $\delta^{18}O$ values with approaching the underlying ductile shear zone (DSZ), in which the eclogites have anomalously light oxygen isotope compositions (Zhang et al., 2006c). Although the oxygen isotope compositions of the eclogite units investigated in this work were obviously affected by the DSZ-associated fluid, most of the data group together and differ from other eclogites, which implies that our samples were formed in a single magmatic event.

The latest SHRIMP U–Pb dating for the inherited zircon cores in the eclogites suggests that protolith age could be 774 Ma (Zhang et al., 2006a). As discussed above, parental materials of the CCSD ultramafic rocks – Mg-rich eclogites–high-Ti eclogites–low-Mg–Ti eclogites probably were peridotite–pyroxenite–garnet gabbro/anorthosite – evolved plutonic rocks, which make up a complete sequence of fractional crystallization. The garnet signatures in the eclogites suggest that some garnets may have an igneous precursor as discussed above. This implies that the gabbro-pyroxenite/peridotite assemblage may have crystallized from a Neoproterozoic basaltic magma chamber in the stability field of garnet, i.e., possibly in the lower crust. These magmas subsequently underwent intermediate pressure fractional crystallization, and later were metamorphosed at UHP conditions during the Triassic continental collision event (Fig. 8).

The assemblage of low-Mg–Ti eclogites+high-Ti eclogites+Mg-rich eclogites+ultramafic rocks could provide a rare window to study fossil lower crust formed by Neoproterozoic basaltic underplating. Mantle-derived, basaltic underplating has been suggested to explain the Neoproterozoic granites (Zhou et al., 2002) that are widely distributed along the margin of the Yangtze Block (Li et al., 1999, 2003a,b; Zhou et al., 2002; Huang et al., 2006). These granites are thought to have been caused by either a mantle plume (Li et al., 1999, 2003a) or formed by arc-related magmatism (Zhou et al., 2002).

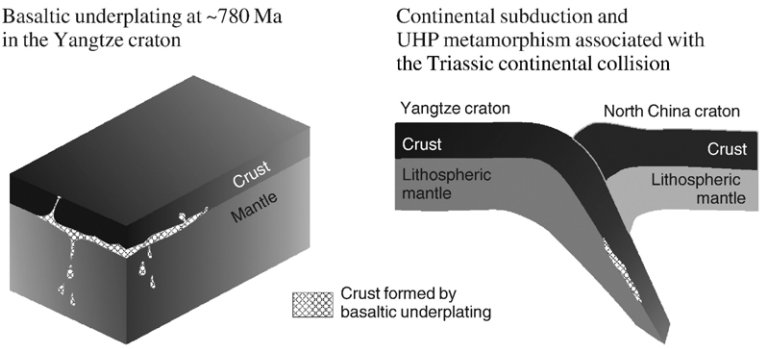

Fig. 8. Cartoon figure illustrating the formation of the eclogite-ultramafic rock assemblage.

Whatever the trigger for granitic magmatism, large-scale lower crustal growth and evolution could have occurred in Neoproterozoic time, as suggested by the widespread occurrence of Neoproterozoic granites (Li et al., 1999, 2003a,b; Zhou et al., 2002; Huang et al., 2006) and mantle-derived igneous rocks (e.g., bimodal volcanics, high-Mg andesites, basalts and gabbros; Li et al., 2002; Ling et al., 2003; Zhao and Zhou, 2007). The significantly variable initial ε_{Nd} values of bimodal volcanics (+1.12 ~ +5.96; Li et al., 2002; −4.9 ~ +5.3; Ling et al., 2003), basalts (+1.7 ~ +10.7; Li et al., 2006) and granites (−0.2 ~ −19.3; Li et al., 2003a), and low initial ε_{Nd} values of olivine gabbros (−0.12 ~ −0.93; Zhao and Zhou, 2007) from these areas indicate that Neoproterozoic underplating of mantle-derived magma could have played an important role in the lower crustal growth and evolution.

6. Conclusions

Except for the highly fluid-mobile elements (e.g., Cs and Pb), compositions of the eclogites from the depth interval of 100–680 of the CCSD-MH were not significantly influenced by UHP metamorphism. LREE enrichments coupled with positive Eu anomalies in serpentinized ultramafic rocks could partially result from serpentinization.

The unusually high $Fe_2O_3^{total}$ and TiO_2 contents and decoupling of high TiO_2 from low Nb (Ta) of the high-Ti eclogites could result from crystal fractionation of titanomagnetite (for those with TiO_2 < ~4 wt.%) or titanomagnetite+ ilmenite (for those with TiO_2 > ~4 wt.%). Their protoliths are probably titanomagnetite/ilmenite-rich gabbroic cumulates. The low-Mg–Ti eclogites are metamorphic products of evolved dioritic cumulates formed by high degrees of crystal fractionation.

As a whole, the remarkable variations of major elements and HFSE and REE of the eclogites and ultramafic rocks are mainly inherited from their magmatic history, and suggest cumulate origins. The eclogites are genetically related to the underlying ultramafic rocks. Parental materials of these eclogites and ultramafic rocks could represent a complete sequence of fractional crystallization of tholeiitic or picritic magmas that formed in the lower crust in Neoproterozoic time, and were later metamorphosed at UHP conditions.

Acknowledgements

We thank Dr. Cin-Ty Lee who provided access to their laboratory in the Rice University. We acknowledge the helpful comments by Dr. Matthias Barth, Othmar Muentener. We also thank Prof. Roberta L. Rudnick and one anonymous reviewer who improve this manuscript significantly. This research is co-supported by the Ministry of Science and Technology of China (2003CB716501), the National Natural Science Foundation of China (40521001, 40473013, 40673026), and the Ministry of Education of China (NCET-05-0664, IRT0441, B07039). Kelemen was supported in part by NSF grants OCE 0426160 and OCE 0405572.

Appendix A. Sample-preparing procedure for ICP-MS analyses

Step	Description
1	~50 mg sample powder was weighed into a Teflon bomb, moistened with a few drops of ultrapure water.
2	1.5 ml HNO_3 + 1.5 ml HF were added. The sealed bomb was heated at 190 °C in oven for 48 h.
3	Open the bomb and evaporate the solution at ~115 °C to dryness. This was followed by adding 1 ml HNO_3 and evaporating to the second round of dryness.
4	The resultant salt was re-dissolved by adding ~3 ml of 30% HNO_3 and resealed and heated in the bomb at 190 °C for 12–24 h.
5	The final solution was diluted to ~100 g with mixture of 2% HNO_3 for ICP-MS analysis.

Appendix B. ICP-MS analyses of international rock standards

Element	HR-ICP-MS analyses at the Rice University						Analyses at the China University of Geosciences						
	LOD	Blank	BHVO2 (n=3)		BIR1 (n=3)		Blank	DNC1		BHVO2		BCR2	
			Average	Stdev	Average	Stdev		Obt.	Ref.	Obt.	Ref.	Obt.	Ref.
V	0.0005	0.9457	329	7.08	346	4.37	0.0900	151	148	306	317	386	416
Cr	0.0034	7.2341	300	6.77	422	13.8	0.1766	292	285	272	280	17.4	18.0
Co	0.0016	0.0887	45.1	0.87	55.4	1.33	0.2904	57.6	54.7	43.5	45	33.8	37.0
Ni	0.0021	2.2585	122	2.33	184	5.66	0.1832	273	247	117	119	11.9	13.0
Cu	0.0017	0.2605	128	1.53	124	5.13	0.2639	74.2	96.0	125	127	21.8	19.0
Zn	0.0028		106	1.74	87.9	19.8	0.5752	52.8	66.0	103	103	110	127
Zr	0.0238	0.5053	178	1.83	16.0	0.54	0.0629	38.3	41.0	172	172	189	188
Nb	0.0017	0.0651	18.1	0.13	0.56	0.04	0.0066	2.73	3.00	18.0	18.0	11.5	13.2
Be	0.0021	0.0283	1.24	0.06	0.11	0.01	0.0039	0.23	1.00	1.11	1.10	2.40	1.60
Ga	0.0001	0.0310	21.1	0.27	14.9	0.32	0.0153	14.3	15.0	21.2	21.7	21.6	23.0
Rb	0.0000	0.0681	8.92	0.16	0.22	0.04	0.2632	5.05	4.50	10.1	9.80	47.1	48.0
Sr	0.0000	0.1244	397	1.38	111	0.85	0.1276	150	145	388	396	322	340
Y	0.0001	0.0109	28.1	0.56	16.9	0.29	0.0075	18.1	18.0	26.0	26.0	33.9	37.0
Cs	0.0001	0.0027	0.10	0.00	0.016	0.021	0.0002	0.30	0.34	0.12	0.13	1.48	1.10
Ba	0.0003	0.3407	131	2.21	7.08	0.62	0.6273	108	114	131	131	661	677
La	0.0001	0.0182	14.6	0.31	0.62	0.03	0.0136	3.86	3.80	15.0	15.2	25.1	24.9
Ce	0.0001	0.0443	37.5	0.00	2.04	0.093	0.0076	8.73	10.6	36.9	37.5	52.4	52.9
Pr	0.0002	0.0023	5.25	0.02	0.37	0.00	0.0041	1.20	1.30	5.34	5.29	6.99	6.57
Nd	0.0009	0.0084	24.4	0.25	2.40	0.01	0.0127	5.44	4.90	23.9	24.5	28.8	28.7
Sm	0.0020	0.0017	6.01	0.10	1.11	0.01	0.0011	1.50	1.38	5.86	6.07	6.19	6.57
Eu	0.0005	0.0006	2.07	0.01	0.53	0.01	0.0017	0.64	0.59	1.99	2.07	1.93	1.96
Gd	0.0005	0.0017	6.14	0.13	1.48	0.15	0.0065	2.03	2.00	6.10	6.24	7.19	6.75
Tb	0.0001	0.0002	0.95	0.00	0.28	0.02	0.0007	0.39	0.41	0.91	0.94	1.04	1.07
Dy	0.0011	0.0015	5.22	0.07	2.14	0.15	0.0047	2.76	2.70	5.25	5.31	6.49	6.41
Ho	0.0003	0.0003	0.97	0.02	0.58	0.01	0.0009	0.67	0.62	0.97	0.97	1.28	1.30
Er	0.0017	0.0011	2.53	0.03	1.74	0.04	0.0000	1.88	2.00	2.44	2.54	3.47	3.66
Tm	0.0003	0.0002	0.33	0.01	0.26	0.00	0.0006	0.31	0.33	0.34	0.34	0.53	0.56
Yb	0.0016	0.0010	2.03	0.03	1.52	0.02	0.0012	2.04	2.01	2.00	2.00	3.42	3.38
Lu	0.0003	0.0002	0.26	0.01	0.23	0.01	0.0000	0.31	0.32	0.28	0.27	0.50	0.52
Hf	0.0004	0.0081	4.18	0.06	0.56	0.00	0.0102	1.03	1.01	4.23	4.10	4.87	4.80
Ta	0.0000	0.1287	1.08	0.10	0.12		0.0229	0.13	0.098	1.30	1.40	0.84	0.78
Pb	0.0000	0.1917	1.49	0.07	3.29	0.51	0.0899	7.09	6.30	2.38	2.60	14.3	11.0
Th	0.0000	0.0066	1.23	0.03	0.029	0.006	0.0186	0.23	0.20	1.14	1.20	6.56	6.20
U	0.0000	0.0020	0.41	0.01	0.010	0.002	0.0035	0.037	0.10	0.42	0.42	1.79	1.69

Units are ppb for blank, and ppm for the others. Obt. = obtained values. Ref. = reference values.
LOD: limit of detection, which was calculated according to 3σ of blank analyses.

References

Agee, C.B., 1990. A new look at differentiation of the Earth from melting experiments on the Allende meteorite. Nature 346, 834–837.

Barth, M.G., Rudnick, R.L., Horn, I., McDonough, W.F., Spicuzza, M.J., Valley, J.W., Haggerty, S.E., 2002. Geochemistry of xenolithic eclogites from West Africa, Part 2: origins of the high MgO eclogites. Geochim. Cosmochim. Acta 66, 4325–4345.

Bebout, G.E., Ryan, J.G., Leeman, W.P., Bebout, A.E., 1999. Fractionation of trace elements by subduction-zone metamorphism-effect of convergent-margin thermal evolution. Earth Planet. Sci. Lett. 171, 63–81.

Becker, H., Jochum, K.P., Carlson, R.W., 2000. Trace element fractionation during dehydration of eclogites from high-pressure terranes and the implications for element fluxes in subduction zones. Chem. Geol. 163, 65–69.

Berger, J., Féménias, O., Coussaert, N., Demaiffe, D., 2005. Magmatic garnet-bearing mafic xenoliths (Puy Beaunit, French Massif Central): P–T path from crystallisation to exhumation. Eur. J. Mineral. 17, 687–701.

Berger, J., Féménias, O., Coussaert, N., Mercier, J.-C.C., Demaiffe, D., 2007. Cumulating processes at the crust-mantle transition zone inferred from Permian mafic-ultramafic xenoliths (Puy Beaunit, France). Contrib. Mineral. Petrol. 153 (5), 557–575.

Bindeman, I.N., Davis, A.M., Drake, M.J., 1998. Ion microprobe study of plagioclase-basalt partition experiments at natural concentration levels of trace elements. Geochim. Cosmochim. Acta 62 (7), 1175–1193.

Bodinier, J.-L., Godard, M., 2003. Orogenic, ophiolitic, and abyssal peridotites. In: Holland, N.D., Turekian, K.K. (Eds.), Treatise on Geochemistry. Elsevier Ltd, pp. 103–170.

Chalot-Prat, F., Ganne, J., Lombard, A., 2003. No significant element transfer from the oceanic plate to the mantle wedge during subduction and exhumation of the Tethys lithosphere (Western Alps). Lithos 69, 69–103.

Chen, R.-X., Zheng, Y.-F., Gong, B., Zhao, Z.-F., Gao, T.-S., Chen, B., Wu, Y.-B., 2007. Oxygen isotope geochemistry of ultrahigh-pressure metamorphic rocks from 200–4000 m core samples of the Chinese Continental Scientific Drilling. Chem. Geol. 242 (1–2), 51–75.

Coogan, L.A., MacLeod, C.J., Dick, H.J.B., Edwards, S.J., Kvassnes, A., Natland, J.H., Robinson, P.T., Thompson, G., O'Hara, M.J., 2001. Whole-rock geochemistry of gabbros from the Southwest Indian Ridge: constraints on geochemical fractionations between the upper and lower oceanic crust and magma chamber processes at very slow-spreading ridges. Chem. Geol. 178, 1–22.

Day, R.A., Green, T.H., Smith, I.E.M., 1992. The origin and significance of garnet phenocrysts and garnet-bearing xenoliths in Miocene calc-alkaline volcanics from Northland, New Zealand. J. Petrol. 33 (1), 125–161.

Desmurs, L., Muntener, O., Manatschal, G., 2002. Onset of magmatic accretion within a magma-poor rifted margin: a case study from the Platta ocean-continent transition, eastern Switzerland. Contrib. Mineral. Petrol. 144 (3), 365–382.

Dunn, T., Sen, C., 1994. Mineral/matrix partition coefficients for orthopyroxene, plagioclase, and olivine in basaltic to andesitic systems: a combined analytical and experimental study. Geochim. Cosmochim. Acta 58, 717–733.

Egorova, V.V., Volkova, N.I., Shelepaev, R.A., Izokh, A.E., 2006. The lithosphere beneath the Sangilen Plateau, Siberia: evidence from peridotite, pyroxenite and gabbro xenoliths from alkaline basalts. Miner. Petrol. 88, 419–441.

El Fadili, S., Demaiffe, D., 1999. Petrology of eclogite and granulite nodules from the Mbuji Mayi kimberlites (Kasai, Congo): significance of kyanite-omphacite intergrowths. In: Gurney, J.J., Gurney, J.L., Pascoe, M.D., Richardson, S.H. (Eds.), Proceedings of the 7th International Kimberlite Conference. Red Roof Design, pp. 205–213.

Enami, M., Nagasaki, A., 1999. Prograde P–T path of kyanite eclogites from Junan in the Sulu ultrahigh-pressure province, eastern China. Isl. Arc 8, 459–474.

Evans, B.W., Trommsdorff, V., Goles, G.G., 1981. Geochemistry of high-grade eclogites and metarodingites from the Central Alps. Contrib. Mineral. Petrol. 76 (3), 301–311.

Foley, S.F., Barth, M.G., Jenner, G.A., 2000. Rutile/melt partition coefficients for trace elements and an assessment of the influence of rutile on the trace element characteristics of subduction zone magmas. Geochim. Cosmochim. Acta 64 (5), 933–938.

Fujimaki, H., 1986. Partition-Coefficients of Hf, Zr, and REE between zircon, apatite, and liquid. Contrib. Mineral. Petrol. 94 (1), 42–45.

Giacomini, F., Braga, R., Tiepolo, M., Tribuzio, R., 2007. New constraints on the origin and age of Variscan eclogitic rocks (Ligurian Alps, Italy). Contrib. Mineral. Petrol. 153 (1), 29–53.

Green, T.H., Pearson, N.J., 1987. An experimental study of Nb and Ta partitioning between Ti-rich minerals and silicate liquids at high pressure and temperature. Geochim. Cosmochim. Acta 51, 55–62.

Greene, A.R., Debari, S.M., Kelemen, P.B., Blusztajn, J., Clift, P.D., 2006. A detailed geochemical study of Island Arc Crust: the Talkeetna Arc Section, South-Central Alaska. J. Petrol. 47 (6), 1051–1093.

Griffin, W.L., O'Reilly, S.Y., 1986. The lower crust in eastern Australia: xenolith evidence. In: Dawson, J.B., Carswell, D.A., Hall, J., Wedepohl, K.H. (Eds.), The Nature of the Lower Continental Crust. Geol. Soc. Spec. Pub. , pp. 363–374.

Griffin, W.L., O'Reilly, S.Y., Pearson, N.J., 1990. Eclogite stability near the crust–mantle boundary. In: Carswell, D.A. (Ed.), Eclogites Facies Rocks. Blackie, pp. 291–314.

Hack, P.J., Nielsen, R.L., Johnston, A.D., 1994. Experimentally determined rare-earth element and Y partitioning behavior between clinopyroxene and basaltic liquids at pressures up to 20 kbar. Chem. Geol. 117, 89–105.

Harangi, S.Z., Downes, H., Kósa, L., Szabó, C.S., Thirlwall, M.F., Mason, P.R.D., Mattey, D., 2001. Almandine garnet in calcalkaline volcanic rocks of the northern Pannonian basin (Eastern–Central Europe): geochemistry, petrogenesis and geodynamic implications. J. Petrol. 42 (10), 1813–1843.

Hart, S.R., Blusztajn, J., Dick, H.J.B., Meyer, P.S., Muehlenbachs, K., 1999. The fingerprint of seawater circulation in a 500-meter section of ocean crust gabbros. Geochim. Cosmochim. Acta 63 (23/24), 4059–4080.

Hermann, J., Muntener, O., Gunther, D., 2001. Differentiation of mafic magma in a continental crust-to-mantle transition zone. J. Petrol. 42 (1), 189–206.

Huang, J., Zheng, Y.-F., Zhao, Z.-F., Wu, Y.-B., Zhou, J.-B., Liu, X., 2006. Melting of subducted continent: element and isotopic evidence for a genetic relationship between Neoproterozoic and Mesozoic granitoids in the Sulu orogen. Chem. Geol. 229, 227–256.

Jahn, B.M., 1998. Geochemical and isotopic characteristics of UHP eclogites and ultramafic rocks of the Dabie Orogen: implications for continental subduction and collisional tectonics. In: Hacker, B.R., Liou, J.G. (Eds.), When Continents Collide: Geodynamics and Geochemistry of Ultrahigh-pressure Rocks. Kluwer Academic Publishers, the Netherlands, pp. 203–239.

Jenner, G.A., Foley, S.F., Jackson, S.E., Green, T.H., Fryer, B.J., Longerich, H.P., 1993. Determination of partition coefficients for trace elements in high pressure–temperature experimental run products by laser ablation microprobe-inductively coupled plasma-mass spectrometry (LAM-ICP-MS). Geochim. Cosmochim. Acta 57 (23–24), 5099–5103.

Johnson, T.M., 1998. Experimental determination of partition coefficients for rare earth and high-field-strength elements between clinopyroxene, garnet, and basaltic melt at high pressures. Contrib. Mineral. Petrol. 133, 60–68.

Kelemen, P.B., 1995. Genesis of high Mg# andesites and the continental crust. Contrib. Mineral. Petrol. 120 (1), 1–19.

Kelemen, P.B., Hanghoj, K., Greene, A.R., 2003. One view of the geochemistry of subduction-related magmatic arcs, with emphasis on primitive andesite and lower crust. In: Rudnick, R.L. (Ed.), The Crust. Treatise on Geochemistry. Elsevier, pp. 593–659.

Kempton, P.D., Harmon, R.S., 1992. Oxygen isotope evidence for large-scale hybridization of the lower crust during magmatic underplating. Geochim. Cosmochim. Acta 56, 971–986.

Kessel, R., Ulmer, P., Pettke, T., Schmidt, M.W., Thompson, A.B., 2005. The water-basalt system at 4 to 6 GPa: phase relations and second critical endpoint in a K-free eclogite at 700 to 1400 °C. Earth Planet. Sci. Lett. 237 (3–4), 873–892.

Klein, M., Stosch, H.G., Seck, H.A., 1997. Partitioning of high field-strength and rare-earth elements between amphibole and quartz-dioritic to tonalitic melts: an experimental study. Chem. Geol. 138 (3–4), 257–271.

Klemme, S., Prowatke, S., Hametner, K., Günther, D., 2005. Partitioning of trace elements between rutile and silicate melts:

implications for subduction zones. Geochim. Cosmochim. Acta 69 (9), 2361–2371.

Lee, C.T.A., Cheng, X., Horodyskyj, U., 2006. The development and refinement of continental arcs by primary basaltic magmatism, garnet pyroxenite accumulation, basaltic recharge and delamination: insights from the Sierra Nevada, California. Contrib. Mineral. Petrol. 151, 222–242.

Lehnert, K., Su, Y., Langmuir, C.H., Sarbas, B., Nohl, U., 2000. A global geochemical database structure for rocks. Geochem. Geophys. Geosyst. 1 Paper number 1999GC000026.

Li, W.-X., Li, X.-H., Li, Z.-X., 2005. Neoproterozoic bimodal magmatism in the Cathaysia Block of South China and its tectonic significance. Precambrian Res. 136 (1), 51–66.

Li, X.-H., Li, Z.-X., Ge, W., Zhou, H., Li, W., Liu, Y., Wingate, M.T.D., 2003a. Neoproterozoic granitoids in South China: crustal melting above a mantle plume at ca. 825 Ma? Precambrian Res. 122 (1–4), 45–83.

Li, X.-H., Li, Z.-X., Sinclair, J.A., Li, W.-X., Carter, G., 2006. Revisiting the "Yanbian Terrane": implications for Neoproterozoic tectonic evolution of the western Yangtze Block, South China. Precambrian Res. 151 (1–2), 14–30.

Li, X.H., Li, Z.X., Zhou, H., Liu, Y., Kinny, P.D., 2002. U–Pb zircon geochronology, geochemistry and Nd isotopic study of Neoproterozoic bimodal volcanic rocks in the Kangdian Rift of South China: implications for the initial rifting of Rodinia. Precambrian Res. 113, 135–155.

Li, Z.X., Li, X.H., Kinny, P.D., Wang, J., 1999. The breakup of Rodinia: did it start with a mantle plume beneath South China? Earth Planet. Sci. Lett. 173, 171–181.

Li, Z.X., Li, X.H., Kinny, P.D., Wang, J., Zhang, S., Zhou, H., 2003b. Geochronology of Neoproterozoic syn-rift magmatism in the Yangtze Craton, South China and correlations with other continents: evidence for a mantle superplume that broke up Rodinia. Precambrian Res. 122, 85–109.

Ling, W., Gao, S., Zhang, B., Li, H., Liu, Y., Cheng, J., 2003. Neoproterozoic tectonic evolution of the northwestern Yangtze craton, South China: implications for amalgamation and break-up of the Rodinia Supercontinent. Precambrian Res. 122 (1–4), 111–140.

Liou, J.G., Carswell, D.A., 2000. Garnet peridotites and ultrahigh-pressure minerals. J. Metamorph. Geol. 18, 121.

Liou, J.G., Zhang, R.Y., 1996. Occurrence of intergranular coesite in Sulu ultrahigh-P rocks from China: implications for fluid activity during exhumation. Am. Mineral. 81, 1217–1221.

Liu, F.L., Xu, Z.Q., Xue, H.M., 2004a. Tracing the protolith, UHP metamorphism, and exhumation ages of orthogneiss from the SW Sulu terrane (eastern China): SHRIMP U–Pb dating of mineral inclusion-bearing zircons. Lithos 78, 411–429.

Liu, F.L., Xu, Z.Q., Yang, J.S., Zhang, Z.M., Xu, H.M., Li, T.F., 2004b. Geochemical characteristics and UHP metamorphism of granitic gneisses in the main drilling hole of Chinese Continental Scientific Drilling Project and its adjacent area. Acta Petrologica Sin. 20 (1), 9–26.

Liu, Q., Hou, Q.L., Zhou, X.H., Xie, L.W., 2005a. The distribution of platinum-group elements in gabbros from Zhujiapu, Dabie orogen. Acta Petrol. Sin. (in Chinese with English Abs.) 21 (1), 227–239.

Liu, Y.-H., Yang, H.-J., Shau, Y.-H., Meng, F., Zhang, J., Yang, J., Xu, Z., Yu, S.-C., 2007a. Compositions of high Fe–Ti eclogites from the Sulu UHP metamorphic terrane, China: HFSE decoupling and protolith characteristics. Chem. Geol. 239, 64–82.

Liu, Y.S., Gao, S., Lee, C.-T.A., Hu, S.H., Liu, X.M., Yuan, H.L., 2005b. Melt–peridotite interactions: Links between garnet pyroxenite and high-Mg# signature of continental crust. Earth Planet. Sci. Lett. 234 (1–2), 39–57.

Liu, Y.S., Hu, Z.C., Gao, S., Zong, K.Q., Gao, C.Q., 2007b. Refining constraints on the UHP metamorphic age of the Sulu terrane by combining zircon trace element analysis and U–Pb dating. Lithos (in review).

Liu, Y.S., Zhang, Z.M., Lee, C.T., Gao, S., Zong, K.Q., 2005c. Decoupled high-Ti from low Nb(Zr) of eclogites from the CCSD: implications for magnetite fractional crystallization in basalt chamber. Acta Petrol. Sin. (in Chinese with English Abs.) 21 (2), 339–346.

Mattinson, C.G., Zhang, R.Y., Tsujimori, T., Liou, J.G., 2004. Epidote-rich talc–kyanite–phengite eclogites, Sulu terrane, eastern China: P–T–fO_2 estimates and the significance of the epidote-talc assemblage in eclogite. Am. Mineral. 89, 1772–1783.

McDonough, W.F., 1990. Constraints on the composition of the continental lithospheric mantle. Earth Planet. Sci. Lett. 101 (1), 1–18.

McDonough, W.F., Sun, S.S., 1995. The composition of the earth. Chem. Geol. 120, 223–253.

McKay, G., Le, L., Wagstaff, J., Crozaz, G., 1994. Experimental partitioning of rare earth elements and strontium: constraints on petrogenesis and redox conditions during crystallization of Antarctic angrite Lewis Cliff 86010. Geochim. Cosmochim. Acta 58 (13), 2911–2919.

McKenzie, D.A.N., O'Nions, R.K., 1991. Partial melt distributions from inversion of rare earth element concentrations. J. Petrol. 32 (5), 1021–1091.

Menzies, M.A., Long, A., Ingram, G., Tatnell, M., Janetzky, D., 1993. MORB peridotite-sea water interaction: experimental constrains on the behaviour of trace elements, $^{87}Sr/^{86}Sr$ and $^{143}Nd/^{144}Nd$ ratios. In: T.A., H.M., Prichard, Harris, N.B.W., Neary, C.R. (Eds.), Magmatic Processes and Plate Tectonics. Geological Society Special Publ. The Geological Society, London, pp. 309–322.

Miller, C., Zanetti, A., Thoni, M., Konzett, J., 2007. Eclogitisation of gabbroic rocks: Redistribution of trace elements and Zr in rutile thermometry in an Eo-Alpine subduction zone (Eastern Alps). Chem. Geol. 239 (1–2), 96–123.

Müntener, O., Kelemen, P.B., Grove, T.L., 2001. The role of H_2O during crystallization of primitive arc magmas under uppermost mantle conditions and genesis of igneous pyroxenites: an experimental study. Contrib. Mineral. Petrol. 141, 643–658.

Müntener, O., Ulmer, P., 2006. Experimentally derived high-pressure cumulates from hydrous arc magmas and consequences for the seismic velocity structure of lower arc crust. Geophys. Res. Lett. 33, L21308.

Nielsen, R.G., Forsythe, L.M., Gallahan, W.E., Fisk, M.R., 1994. Major- and trace-element magnetite-melt equilibria. Chem. Geol. 117 (1–4), 167–191.

Nielsen, R.L., Beard, J.S., 2000. Magnetite-melt HFSE partitioning. Chem. Geol. 164, 21–34.

Paster, T.P., Schauwecker, D.S., Haskin, L.A., 1974. The behavior of some trace elements during solidification of the Skaergaard layered series. Geochim. Cosmochim. Acta 38 (10), 1549–1577.

Paulick, H., Bach, W., Godard, M., De Hoog, J.C.M., Suhr, G., Harvey, J., 2006. Geochemistry of abyssal peridotites (Mid-Atlantic Ridge, 15°20'N, ODP Leg 209): implications for fluid/rock interaction in slow spreading environments. Chem. Geol. 234 (3–4), 179–210.

Pertermann, M., Hirschmann, M.M., 2003a. Anhydrous partial melting experiment on MORB-like eclogites phase relations, phase composition and mineral-melt partitioning of major elements at 2–3 GPa. J. Petrol. 44, 2173–2202.

Pertermann, M., Hirschmann, M.M., 2003b. Partial melting experiments on a MORB-like pyroxenite between 2 and 3 GPa: constraints on the presence of pyroxenites in basalt source regions. J. Geophys. Res. 108 (B2), 2125. doi:10.1029/2000JB000118.

Prowatke, S., Klemme, S., 2006. Trace element partitioning between apatite and silicate melts. Geochim. Cosmochim. Acta 70 (17), 4513–4527.

Rapp, R.P., Shimizu, N., Norman, M.D., Applegate, G.S., 1999. Reaction between slab-derived melts and peridotite in the mantle wedge: experimental constraints at 3.8 GPa. Chem. Geol. 160, 335–356.

Reynolds, I.M., 1985. The nature and origin of titaniferous magnetite-rich layers in the upper zone of the Bushveld complex: a review and synthesis. Economic Geology 80, 1089–1108.

Ringuette, L., Martignole, J., Windley, B.F., 1999. Magmatic crystallization, isobaric cooling, and decompression of the garnet-bearing assemblages of the Jijal sequence (Kohistan terrane, western Himalayas). Geology 27 (2), 139–142.

Rudnick, R.L., 1992. Xenoliths-samples of the lower continental crust. In: R.A.a., D.M., R.W.K., Fountain (Eds.), Continental Lower Crust. Elsevier, pp. 269–316.

Rudnick, R.L., 1995. Making continental crust. Nature 378, 571–578.

Rudnick, R.L., Gao, S., Ling, W.L., Liu, Y.S., McDonough, W.F., 2004. Petrology and geochemistry of spinel peridotite xenoliths from Hannuoba and Qixia, North China craton. Lithos 77, 609–637.

Rudnick, R.L., McDonough, W.F., McCulloch, M.T., Taylor, S.R., 1986. Lower crust xenoliths from Queensland, Australia:Evidence for deep crustal assimilation and fractionation of continental basalts. Geochim. Cosmochim. Acta 50, 1099–1115.

Salters, V., Stracke, A., 2004. Composition of the depleted mantle. Geochem. Geophys. Geosyst. 5 (5), Q05004. doi:10.1029/2003GC000597.

Scambelluri, M., Rampone, E., Piccardo, G.B., 2001. Fluid and element cycling in subducted serpentinite: A trace element study of the Erro–Tobbio high-pressure ultramafites (Western Alps, NW Italy). J. Petrol. 42 (1), 55–67.

Schmidt, M.W., Dardon, A., Chazot, G., Vannucci, R., 2004. The dependence of Nb and Ta rutile-melt partitioning on melt composition and Nb/Ta fractionation during subduction processes. Earth Planet. Sci. Lett. 226 (3–4), 415–432.

Scribano, V., Sapienza, G., Braga, R., Morten, L., 2006. Gabbroic xenoliths in tuff-breccia pipes from the Hyblean Plateau: insights into the nature and composition of the lower crust underneath South-eastern Sicily, Italy. Miner. Petrol. 86, 63–88.

Snow, J.E., Dick, H.J.B., 1995. Pervasive magnesium loss by marine weathering of peridotite. Geochim. Cosmochim. Acta 59 (20), 4219–4235.

Spandler, C., Hermann, J., Arculus, R., Mavrogenes, J., 2004. Geochemical heterogeneity and element mobility in deeply subducted oceanic crust; insights from high-pressure mafic rocks from New Caledonia. Chem. Geol. 206 (1–2), 21–42.

Tang, H.-F., Liu, C.-Q., Nakai, S.I., Orihashi, Y., 2007. Geochemistry of eclogites from the Dabie–Sulu terrane, eastern China: new insights into protoliths and trace element behaviour during UHP metamorphism. Lithos 95 (3–4), 441–457.

Toplis, M.J., Carroll, M.R., 1996. Differentiation of ferro-basaltic magmas under conditions open and closed to oxygen: implications for the Skaergaard intrusion and other natural systems. J. Petrol. 37 (4), 837–858.

Ulmer, P., 1989. Partitioning of high-field strength elements among olivine, pyroxenes, garnet and calc–alkaline picrobasalt; experimental results and an application. Ann. Rep. Director Geophys. Lab. Carnegie Inst, Washington, pp. 42–47. 1988–1989.

Villiger, S., Ulmer, P., Muntener, O., Thompson, A.B., 2004. The liquid line of descent of anhydrous, mantle-derived, tholeiitic liquids by fractional and equilibrium crystallization—an experimental study at 1.0 GPa. J. Petrology 45 (12), 2369–2388.

Wendlandt, E., DePaolo, D.J., Baldridge, W.S., 1993. Nd and Sr isotope chronostratigraphy of Colorado Plateau lithodphere: implications for magmatic and tectonic underplating of the continental crust. Earth Planet. Sci. Lett. 116, 23–43.

Workman, R.K., Hart, S.R., 2005. Major and trace element composition of the depleted MORB mantle (DMM). Earth Planet. Sci. Lett. 231 (1–2), 53–72.

Xiong, X.L., Adam, T.J., Green, T.H., 2005. Rutile stability and rutile/melt HFSE partitioning during partial melting of hydrous basalt: implications for TTG genesis. Chem. Geol. 218, 339–359.

Xu, J., Chen, Y.C., Wang, D.H., Yu, J.J., Li, C.J., Fu, X.J., Chen, Z.Y., 2004a. Titanium mineralization in the ultrahigh-pressure metamorphic rocks from Chinese Continental Scientifc Drilling 100–2000 m main hole. Acta Petrol. Sin. (in Chinese with English Abs.) 20 (1), 119–126.

Xu, S.T., Liu, Y.C., Chen, G.B., Roberto, C., Franco, R., He, M.C., Liu, H.F., 2003. New finding of microdiamonds in eclogites from Dabie–Sulu region in central-eastern China. Chin. Sci. Bull. 48 (10), 988–994.

Xu, Z.Q., Zhang, Z.M., Liu, F.L., Yang, J.S., Tang, Z.M., Cheng, S.Z., Cai, Y.C., Li, T.F., Cheng, F.Y., 2004b. The structure profile of 0–1200 m in the main borehole, Chinese Continental Scientific Drilling and its preliminary deformation analysis. Acta Petrol. Sin. (in Chinese with English Abs.) 20 (1), 53–72.

Yang, J.J., Jahn, B.M., 2000. Deep subduction of mantle-derived garnet peridotites from the Su-Lu UHP metamorphic terrane in China. J. Metamorph. Geol. 18 (2), 167–180.

Yaxley, G.M., 2000. Experimental study of the phase and melting relations of homogeneous basalt+peridotite mixtures and implications for the petrogenesis of flood basalts. Contrib. Mineral. Petrol. 139, 326–338.

Zack, T., Brumm, R., 1998. Ilmenite/liquid partition coefficients of 26 trace elements determined through ilmenite/clinopyroxene partitioning in garnet pyroxene. In: Gurney, J.J., Gurney, J.L., Pascoe, M.D., Richardson, S.H. (Eds.), Proceedings of the 7th International Kimberlite Conference. Red Roof Design, Cape Town, pp. 986–988.

Zhang, R.Y., Zhai, M.G., Fei, Y.W., Liu, J.G., 2003. Titanium solubility in coexisting garnet and clinopyroxene at very high pressure: the significance of exsolved rutile in garnet. Earth Planet. Sci. Lett. 216, 591–601.

Zhang, Z.M., Liou, J.G., Zhao, X.D., Shi, C., 2006a. Petrogenesis of Maobei rutile eclogites from the southern Sulu ultrahigh-pressure metamorphic belt, eastern China. J. Metamorph. Geol. 24, 727–741.

Zhang, Z.M., Xiao, Y.L., Hoefs, J., Liou, J.G., Simon, K., 2006b. Ultrahigh pressure metamorphic rocks from the Chinese Continental Scientific Drilling Project: I. Petrology and geochemistry of the main hole (0–2,050 m). Contrib. Mineral. Petrol. 152, 421–441.

Zhang, Z.M., Xiao, Y.L., Zhao, X.D., Shi, C., 2006c. Fluid-rock interaction during the continental deep subduction: Oxygen isotopic profile of the main hole of the CCSD project. Acta Petrol. Sin. 22 (7), 1941–1951.

Zhang, Z.M., Xu, Z.Q., Liu, F.L., You, Z.D., Shen, K., Yang, J.S., Li, T.F., Chen, S.Z., 2004. Geochemistry of eclogites from the main hole (100–2050 m) of the Chinese Continental Scientific Drilling

Project. Acta Petrol. Sin. (in Chinese with English Abs.) 20 (1), 27–42.

Zhang, Z.M., Xu, Z.Q., Xu, H.F., 2000. Petrology of ultrahigh-pressure eclogites from the ZK703 drillhole in the Donghai, eastern China. Lithos 52, 35–50.

Zhao, J., Zhou, M., 2007. Geochemistry of Neoproterozoic mafic intrusions in the Panzhihua district (Sichuan Province, SW China): Implications for subduction-related metasomatism in the upper mantle. Precambrian Res. 152, 27–47.

Zhou, C.Y., Wu, F.Y., Ge, W.C., Sun, D.Y., Abdel, R.A.A., Zhang, J.H., Cheng, R.Y., 2005a. Age, geochemistry and petrogenesis of the cumulate gabbro in Tahe, northern Da Hinggan Mountain. Acta Petrol. Sin. (in Chinese with English Abs.) 21 (3), 763–775.

Zhou, M.-F., Robinson, P.T., Lesher, C.M., Keays, R.R., Zhang, C.-J., Malpas, J., 2005b. Geochemistry, petrogenesis and metallogenesis of the Panzhihua Gabbroic layered intrusion and associated Fe–Ti–V oxide deposits, Sichuan Province, SW China. J. Petrol. 46 (11), 2253–2280.

Zhou, M.-F., Yan, D.-P., Kennedy, A.K., Li, Y., Ding, J., 2002. SHRIMP U–Pb zircon geochronological and geochemical evidence for Neoproterozoic arc-magmatism along the western margin of the Yangtze Block, South China. Earth Planet. Sci. Lett. 196, 51–67.